

Modeling competing endogenous RNAs networks

Carla Bosia^{1*}, Andrea Pagnani¹, Riccardo Zecchina^{1,2}

1 The Human Genetics Foundation (HuGeF), Via Nizza 52, I-10126, Torino, Italy.

2 Physics Department and Center for Computational Sciences, Politecnico Torino, Corso Duca degli Abruzzi 24, 10129, Torino, Italy.

* E-mail: carla.bosia@hugef-torino.org

Abstract

MicroRNAs (miRNAs) are small RNA molecules, about 22 nucleotide long, which post-transcriptionally regulate their target messenger RNAs (mRNAs). They accomplish key roles in gene regulatory networks, ranging from signaling pathways to tissue morphogenesis, and their aberrant behavior is often associated with the development of various diseases. Recently it has been shown that, in analogy with the better understood case of small RNAs in bacteria, the way miRNAs interact with their targets can be described in terms of a titration mechanism characterized by threshold effects, hypersensitivity of the system near the threshold, and prioritized cross-talk among targets. The latter characteristic has been lately identified as competing endogenous RNA (ceRNA) effect to mark those indirect interactions among targets of a common pool of miRNAs they are in competition for. Here we analyze the equilibrium and out-of-equilibrium properties of a general stochastic model of M miRNAs interacting with N mRNA targets. In particular we are able to describe in details the peculiar equilibrium and non-equilibrium phenomena that the system displays around the threshold: (i) maximal cross-talk and correlation between targets, (ii) robustness of ceRNA effect with respect to the model's parameters and in particular to the catalyticity of the miRNA-mRNA interaction, and (iii) anomalous response-time to external perturbations.

Introduction

A recently discovered molecular mechanism [1], lately named Competing Endogenous RNA (ceRNA) effect [2,3], points out the importance of indirect interactions among transcript RNAs in competition for the same pool of microRNAs (miRNAs). MiRNAs are small – about 22 nucleotide long – non-coding RNAs which post-transcriptionally interact with their targets in a sequence dependent manner. In their mature stage, miRNAs get included in a RNA-induced silencing complex (RISC) and, eventually, thanks to a 6-8 nucleotide long seed region, bind specifically the miRNA response elements (MREs) in the 3'UTR of their target mRNAs. Depending on the degree of complementarity of the seed region, miRNAs can either cleave the transcripts (large overlap with the target) or downregulate their translation (low overlap with the target): in either case the net effect is a reduced amount of mRNAs or proteins. MiRNAs are known to regulate a multitude of different processes ranging from differentiation to neural plasticity, and their malfunctioning is often associated with the development of diseases [4,5].

In a nutshell the idea behind the ceRNA effect boils down to the simple observation that, while interacting with a target mRNA, a single miRNA cannot act on other targets. Mature miRNAs (*i.e.* miRNAs loaded in RISC) are thus the limiting factor in a system of potentially interacting target mRNAs. If for example gene A which shares one miRNA with gene B, is up-regulated the common miRNAs will tend to bind preferentially to mRNA A due to its increased concentration. Consequently, mRNA of gene B will be less repressed resulting in a subsequent increased concentration [1–3, 6, 7]. Other studies have independently provided further evidences for miRNA mediated trans-regulatory mRNA effects [8, 9]. Since each miRNA can have several targets, a complex indirect interaction network among different targets emerges, where nodes are mRNA transcripts and there is a link between two nodes if they have at least one miRNA in common. Then, the highest the number of common miRNAs or MREs, the strongest the link. Such crosstalk effect has been observed in bacteria where the role of miRNAs is played by

small RNAs (sRNAs) and it is due to a titrative interaction among sRNAs and targets [10]. Depending on the number of sRNA binding elements crosstalk among sRNA targets can then be prioritized and selective [10, 11].

Interaction via titration mechanisms entails a threshold-like behavior between the two interacting molecules, where the threshold position is determined by the relative amount of them [10, 12–15]. This means that as long as the concentration of one of these two molecules is below the threshold almost all of them are bound in complexes with the second ones and their free amount is very low. Increasing their concentration beyond the threshold results in an increased amount of free molecules, while the others will be in turn almost all bound in complexes. Moreover, systems of molecules interacting in a titrative fashion also show a hypersensitivity in proximity to the threshold to changes in the molecule production rates [12, 13]. In particular controlled conditions it has been shown that it is right near the threshold, where sensitivity is maximal, that crosstalk among sRNA targets is maximal too [10].

Remarkably, Mukherji and co-workers [16] recently observed a threshold-like effect also in miRNA target expression in single cells. Moreover, in line with studies in bacteria [10, 14] and with earlier works on protein-protein interaction [12, 13], they tested a mathematical deterministic model of molecular titration to describe their results and found it in good agreement with experimental observations. Such results strengthen the idea that behind the ceRNA effect there is a miRNA-target titration mechanism.

Motivated by [16] and [2, 3] and by results obtained in experiments with bacteria [10, 11, 14], in this paper we extend previous models to the case of a general network of M miRNAs titratively interacting with N target mRNAs (ceRNAs) and analyze it from a stochastic point of view. So far analytical predictions from models for titrative interactions did not go beyond the mean-field limit [10, 14, 16] or were limited to the case of small circuits because of the nonlinearities involved [12]. However, (i) stochasticity plays a central role in gene expression mostly when numbers of molecules involved are modest [17–19] and (ii) small circuits are usually embedded in more complex networks so that induced interactions might be relevant. Since potential crosstalk among miRNA targets is effective right in proximity to the threshold, where free chemical species (*i.e.* not bound in complexes) are present in small numbers, it is necessary a stochastic analysis of the system.

Here we show that, despite the complexity and the intrinsic non-linearity of the system, a shrewd use of the moment generating function approach plus a simple Gaussian approximation are enough to obtain analytical expressions for noise and Pearson’s correlation coefficients for all the molecular species considered in a generic network.

As a preliminary result we describe, at the level of the independent molecular species approximation (*viz.* mean-field), the onset of a threshold-like behavior typical of titration mechanism [10, 12–15], which has been specifically investigated in [20] in the case of a miRNA-mediated mRNA interaction, and discuss the possible mechanism leading to a specificity of the interactions.

Secondly, for the first time, we derive analytical results beyond the independent molecular species approximation which allows for the characterization of profiles for means, noise and Pearson’s correlation coefficients, comparing them with numerical simulations. Interestingly, we found that in proximity to the threshold both noise and correlation profiles among the different molecular species (in terms of Fano factor and coefficient of variation) show a maximum. Titration-like interactions could thus be an adequate mechanism to maintain homeostasis in the system: even if the noise increases, ceRNAs or miRNAs fluctuate in a highly correlated manner as discussed in [21–23].

Among the different parameters characterizing miRNA-mRNA interactions, the degree of catalyticity – *i.e.* the fraction of mRNA molecules that are recycled after the interaction with their target – is among the most disputed yet less understood ones: [24, 25] support an almost completely catalytic interaction ($\alpha \sim 0$), while at the opposite range [26–28] support an almost completely stoichiometric interaction ($\alpha \simeq 1$). Finally, intermediate values of catalyticity are indeed supported by a recent work [29]. Here we show that ceRNA effect is robust with respect to this parameter too. In the limiting case of a completely catalytic interaction (*i.e.* 100% of the miRNA is recycled) a threshold-behavior is still observed as an

intrinsically out-of-equilibrium phenomenon: the location of the threshold turns out to be a monotonously increasing function of time such that, at equilibrium (long-time limit), no threshold behavior is observed.

An out-of-equilibrium characteristic of the system predicted by the model is the response time of a ceRNA embedded in a network after a single factor perturbation. Again, in proximity to the threshold, we observe peculiar trends: upon switching on or off another ceRNA in the network the response times show a maximum and a minimum respectively, and the qualitative profiles are independent of the number of ceRNAs in competition.

Finally we conclude proposing a series of specific experiments aiming at validating both qualitatively and quantitatively the model's predictions.

Results

Definition of a network of interaction miRNAs-ceRNAs

The network we are interested in describing is schematically depicted in Figure 1A, where M different free mature miRNAs (colored stars) can interact with N different free target mRNAs (colored pentagons). miRNAs and target mRNAs interact via a titration-like mechanism [16]. As a first approximation we can think the mRNAs as irreversibly lost due to the miRNAs actions (miRNA-target association rate much greater than dissociation rate) while the miRNAs can eventually be recycled. Figure 1B shows a cartoon of such mechanism in which two different DNA molecules (green rectangles) are transcribed with rates k_{S_i} and k_{R_j} to become miRNA S_i and mRNA R_j respectively. Eventually S_i and R_j either degrade (broken gray stars and pentagons) with rates g_{S_i} and g_{R_j} or interact binding in a complex C_{ij} via an effective association rate g_{ij} .

The effective association rate g_{ij} should be thought as a combination of association, dissociation and degradation rates of the miRNA-mRNA complex C_{ij} (see SI for more details). Once in the complex the mRNA R_j cannot be translated or utilized anymore. The parameter α (with $0 \leq \alpha \leq 1$) is a measure of the catalyticity of the miRNA, that is the ability the miRNA has to be available again once having interact with its target. Thus, $\alpha = 1$ means that for each mRNA R_j bound in a complex C_{ij} there is also one miRNA S_j sequestered (and no more able to interact with its other targets) while $\alpha = 0$ implies that mRNA R_j effective degradation is increased by g_{ij} but this does not have any effect on the miRNA S_i .

Mean field approximation: threshold behavior and cross-talk

The onset of a threshold-like response as a consequence of a titration mechanism is a rather well known phenomenon [10, 12–16, 20]. In Figures 2A and 3A, we show an example of threshold effect in the case $M = N = 2$ as a function of different ceRNA and miRNA concentrations. Such an effect can be derived under the assumption that the joint probability distributions of the different molecular species are statistically independent, as explained in Section *Materials and Methods*.

In a general network of interaction of N ceRNAs and M miRNAs, when miRNA-target interaction strength is high, following the derivation of Eq. 11 and depending on the control parameter we decide to tune, two distinct phases emerge: (i) if all target transcription rates are below the threshold level, explicitly computable in terms of all other model's parameters, all targets turn out to be bounded in complexes and the free molecule (*i.e.* not bounded) share is very low, (ii) if at least one of the transcription rate – say the q -th target – is above threshold, then all other target free molecule shares are expressed in finite amount. As shown in Figure 2A, the emerging scenario entails a cross-talk mechanism where a single mRNA target above threshold is able to drive the other common mRNA targets above threshold. The hypothesis of a strong ceRNA-miRNA interaction can be relaxed, and still, a smoother threshold-like behavior is observed [10].

Interestingly enough we note that if, as control parameter, we decide to tune the p -th miRNA transcription rate, keeping all the remaining model's parameters fixed, a mirror-like scenario emerges (as displayed in Figure 3A): in complete analogy with the case previously discussed, also miRNAs cross-talk through ceRNAs. Here again, as long as all miRNAs transcription rates are below threshold, free miRNA molecule shares are very low. As the first miRNA transcription rate crosses the threshold, all other miRNAs show a substantial increase of their free share. In this case too there is a clear cross-talk between miRNAs. It is interesting to note that the threshold value predicted by the model (see section *Materials and methods*) occurs at near-equimolar concentrations of the different chemical species.

If a hierarchy is present for the miRNA-target interaction strengths $g_{ij}/(g_{R_i}g_{S_j})$ [10, 20], for example accounting for different miRNA regulatory elements (MREs) for different target mRNAs, then a hierarchy will be also established in the other target (miRNA) signal amplification levels when the amount of target mRNAs (miRNAs) is moved from below to above the threshold value. Targets sharing similar MREs will be more co-regulated than targets sharing only few MREs [20]. The miRNA-target interplay may thus be selective depending on the particular affinities and binding strengths [10, 11]. This leads to a complex regulatory network with non-trivial indirect interactions among targets in competition for the same pool of miRNAs.

The network sketched in Figure 1A is a crude simplification of what should be a real-case ceRNA's network. To make things slightly more realistic see Figure 4A, where two groups of ceRNAs interact through two distinct sets of miRNAs [20]. However, a small subset of miRNAs makes the two groups of ceRNAs, otherwise statistically independent, *weakly interacting* by cross-connecting the two sets. We simulated the network's dynamics using the Gillespie algorithm in two different settings: in the first one, we modulate over time the transcription rate of one ceRNA, starting with a value below threshold and we first increase the transcription of one specific ceRNA (ceRNA1) rate after 35 hours. A first observation is that it is enough to bring above threshold a single ceRNA, to set the whole network in its non-repressed state. The second observation is that ceRNA-mediated regulation can be specific, *i.e.* we observe a clear hierarchy in the response of the different ceRNAs (see Figure 4B): those ceRNAs sharing the largest set of miRNA (red pentagons) respond more than the yellow pentagon set that shares a fewer number of ceRNAs. A second increase in the transcription rate of ceRNA1 after 70 hours makes the hierarchy in the responses even more clear. Interestingly, also the sets of ceRNAs (orange and blue pentagons) which do not share any targeting miRNA respond to the over-expression of ceRNA1 (although less than the previous two groups), thanks to an undirected effective interaction: ceRNA1 pulls up the red and yellow pentagon sets, the yellow pentagon set pulls up the orange, and the latter the blue pentagon set.

In the second setting (see Figure 4C), we analyze the mirror scenario in which miRNA10 transcription rate is increased. Again the hierarchical responses of the different miRNAs is clearly visible.

Beyond mean field approximation: noise and correlation coefficients

To get insight into molecular species correlations for the miRNA-ceRNA interaction network we then assume that the joint probability distribution P for the different molecular species is a multivariate Gaussian (see section Materials and Methods). This *ansatz* turns out to be useful since all moments of a multivariate Gaussian can be expressed as a function of the first two, *i.e.* in terms of means and covariances. We will assume that the vector $\vec{X} = (X_1, \dots, X_{N+M}) := (R_1, \dots, R_N, S_1, \dots, S_M)$ is distributed according a Gaussian multivariate measure of mean $\mu_i := E(X_i)$ and covariances $c_{ij} := E(X_i X_j) - E(X_i)E(X_j)$. Thus the generic third and fourth moments read $E(X_i X_j X_k) := c_{ij}\mu_k + c_{ik}\mu_j + c_{jk}\mu_i$ and $E(X_i X_j X_k X_l) := c_{ij}c_{kl} + c_{ik}c_{jl} + c_{il}c_{jk}$.

In this way we are able to obtain a closed system of equations for $\langle X_i \rangle$, $\langle X_i^2 \rangle$ and $\langle X_i X_j \rangle$ (see Supplementary Material for a detailed analysis). This assumption is not arbitrary (the usual van Kampen's expansion method [30] shows the master equation is Gaussian except for small corrections) and interestingly performs better than the most widely used linear noise approximation (see Supplementary Materials) when compared with Gillespie's simulations (see [31] for a nice introduction to the subject).

Under this approximation we then find an analytical expression for means, noise and Pearson’s correlation coefficients.

The threshold is characterized not only by the abrupt change of the mean quantities as a function of the control parameter, but also by Pearson’s correlation coefficients and noise (both related to the covariances) which turn out to show a maximum around the threshold. For each molecular species we evaluated in terms of variance $\sigma_{\langle x_i \rangle} := \sqrt{\langle X_i^2 \rangle - \langle X_i \rangle^2}$ the Fano factor, $f_{x_i} = \sigma_{\langle x_i \rangle}^2 / \langle x_i \rangle$, and the coefficient of variation, $CV_{x_i} = \sigma_{\langle x_i \rangle} / \langle x_i \rangle$, which are both measures of noise. While the first one tells how much a particular process is different from a Poisson process, the second is a dispersion index. Figures 2B,C and 2B,C show such noise profiles as a function of ceRNA1 or miRNA1 transcription rate. As it is possible to notice in Figures 2B and 3B, in proximity to the threshold the joint probability distributions are far from being independent ($f_{x_i} \gg 1$ for all indexes i labelling the different chemical species) while a multivariate Gaussian approximation is better suited to describe the simulation results. In Figures 2C and 3C we plot the CV profiles. Increasing the ceRNA1 (miRNA1) transcription rate we observe a decreasing noise profile for ceRNAs (miRNAs) and an increasing one for miRNAs (ceRNAs), as expected because of the increasing and decreasing amount of free ceRNAs (miRNAs) and miRNAs (ceRNAs) respectively. Interestingly, right close to the threshold it is possible to notice a bump in the CV profiles. This phenomenon, due to the variances growing faster than means, is compatible with the bimodal distributions experimentally observed and verified via simulations in particular controlled conditions in bacterial sRNA target [32,33].

The Pearson’s correlation coefficients, $\rho_{X_i, X_j} = \frac{\langle x_i x_j \rangle - \langle x_i \rangle \langle x_j \rangle}{\sigma_{\langle x_i \rangle} \sigma_{\langle x_j \rangle}}$, are shown in Figures 2D and 3D. The profile of the curves as a function of the control parameter, with a well-defined maximum, confirms the system hypersensitivity near the threshold. Analogously, we can define the Pearson correlation coefficient between miRNAs and ceRNAs (not shown). In this case, miRNAs and ceRNAs are negatively correlated.

It is interesting to notice that exactly where the number of interacting molecules is small and the noise profiles show local maxima, the statistical correlation between molecular species is maximal too. Speculatively, the titration interaction mechanism provides for a tool able to maintain the network homeostasis: potentially interacting ceRNAs (or miRNAs) needed in the same time fluctuate together .

Threshold effect and miRNA-target catalytic interaction

So far we considered a titrative stoichiometric ($0 < \alpha \leq 1$) ceRNA/miRNA interaction. However, the open question is if cross-talk among miRNAs or miRNA targets can be possible in case of purely catalytic-like interaction (that is, in case of complete miRNA recycling, or rather $\alpha = 0$ in Equation 1) [28].

It is straightforward to see that, at the steady state, equations for the various $\langle R_j \rangle$ (or $\langle S_i \rangle$) decouple when $\alpha = 0$ (see Equation 10) [20]. As a consequence, no cross-talk is possible among ceRNAs (or miRNAs). We found that in the out of equilibrium phase instead, the behavior is different.

We considered the time evolution of the system in Equation 1 of the Supplementary Material, and then took pictures of the system at a given time t . If t is sufficiently small with respect to the time the complexes need to reach the steady-state, for different values of miRNA (or ceRNA) transcription rate we can observe the threshold behavior of Figure 5A. Consequently ceRNAs or miRNAs cross-talk is possible, and statistical correlations are maximal, as shown by the Pearson’s correlation coefficient profile in Figure 5B.

The emerging picture is that of a dynamical threshold whose value at a given time t tends monotonously to the equilibrium one in case of $\alpha \neq 0$ and to infinity in case of $\alpha = 0$ for large time. In the latter case no cross-talk is observed at equilibrium (Figure 5C,D).

The ceRNA effect is therefore robust also in case of catalytic miRNA-target interaction, the crucial point lying in the instant of time at which we look at the system.

Response times

We have already discussed the threshold effect due to titrative miRNA-target interaction and how the system displays strong sensitivity (maximum cross-talk) and the maximal statistical correlation. We now want to understand how fast the system responds to an external perturbation. In particular we want to compute the time needed for a particular ceRNA (say ceRNA1) to reach the equilibrium after the instantaneous over-expression or knock-out of a second ceRNA (ceRNA2).

Following [34], we consider two different settings: (i) to mimic a sudden signal which saturates ceRNA2 promoter at $t = 0$, the transcription rate k_{R_2} of ceRNA2 switches from zero to a given value (ceRNA2_{OFF→ON}), (ii) to mimic the opposite condition of a sudden drop of the activating signal at $t = 0$, the transcription rate of ceRNA2 k_{R_2} switches from its initial value to zero (ceRNA2_{ON→OFF}).

Defining the response time as the time needed to reach half of the way between initial and final ceRNA1 steady state, we evaluate the response times for both switch-on (T_{ON}) and switch-off (T_{OFF}) (*i.e.* for ceRNA2_{OFF→ON} and ceRNA2_{ON→OFF} respectively) conditions. We integrated numerically the deterministic system of equations obtained with $M = 1$ and $N = 2$ (see Equation 2 in Supplementary Material) to calculate: (i) the time T_{ON} such that $R_1(T_{\text{ON}}) = R_{1_0} + (R_{1_{ss}} - R_{1_0})/2$ (where R_{1_0} and $R_{1_{ss}}$ are the initial and final ceRNA1 steady-state respectively), (ii) the time T_{OFF} such that $R_1(T_{\text{OFF}}) = R_{1_0} - (R_{1_0} - R_{1_{ss}})/2$. The initial conditions are $R_2(0) = 0$ and $R_1(0)$ and $S(0)$ with their steady state values in absence of R_2 in the former case, and $R_2(0) \neq 0$ and $R_1(0)$ and $S(0)$ with their steady state values in presence of R_2 in the latter. We also considered a slightly more complex network in which more ceRNAs are present and we compute ceRNA1 response time with $N = 5, 10, 20$.

We then ask two questions: (i) how the response time of ceRNA1 changes at different values of basal miRNA concentration, and (ii) what happens when the system is complicated by the addition of other competing targets.

As displayed in Figure 6A,B, upon increasing miRNA transcription rate ceRNA1 T_{ON} and T_{OFF} show a maximum and a minimum respectively. Both the maximum and the minimum are located at the threshold, where ceRNA1 initial and final equilibrium values are near (see Figure 6C). Such response time trend suggests an *out-of-equilibrium phase transition*, for which the system experiences anomalous dynamical features around threshold. Let us point out that around threshold, despite the change in terms of number of molecules from initial and final steady state is small, as depicted in Figure 6C, T_{ON} is largely increased while T_{OFF} is decreased. Moreover, the qualitative shape of the curve is robust with respect to the number of targets in competition for the same miRNA (see Figure 6A,B where different line colors correspond to a different number of ceRNAs in the interaction's network): the maximum (resp. the minimum) of the response time depends only mildly on the number of ceRNA competitors, whereas the location of the threshold at which the free molecule share of ceRNA1 starts being repressed depends linearly on the number of competitors. Moreover, the statistical correlation between ceRNA1 and ceRNA2 seems independent from the size of the ceRNA's network: the maximum level of correlation is almost the same upon increasing the number of ceRNAs with only a shift to higher miRNA transcription rates (Figure 6D). Therefore ceRNA1 and ceRNA2 are always very correlated, notwithstanding the dynamical anomalies in the response-time around threshold.

Discussion

In this paper we analyzed the theoretical framework for the stochastic description of a general network of M miRNAs interacting with N target mRNAs via a titration mechanism. With a dexterous use of the moment generating function approach plus simple Gaussian approximation we showed that it is possible to obtain analytical expressions for means and covariances for all the interacting molecules present in the system.

We have first shown how the already well understood threshold effect implied by titrative interac-

tion [10, 12–15] entails with interesting cross-talk phenomena which, so far, have been only partially investigated from the experimental point of view [1–3, 7–9]. In particular the issue of the mirror scenario – for which not only ceRNAs cross-talk through competing for the same set of miRNAs, but, symmetrically the same set of miRNAs too cross-talk through the common set of ceRNA – is a straightforward verification of the *ceRNA hypothesis* which, at the best of our knowledge, has never been attempted so far. In practice, knowing the set of miRNAs belonging to a specific ceRNA network, one could knock-down (resp. over-express) a given miRNA in the network. In this case, the model predicts that the other miRNAs in the network, driven by the controlled miRNA knock-down (resp. over-expression), should increase (resp. decrease) their free molecule share. Such an effect could be directly measurable as a down-regulation (resp. up-regulation) of any of the miRNAs targets (either belonging to the same ceRNA network, or to any other secondary target).

In addition to cross-talk and threshold phenomena, the model predicts interesting and experimentally measurable trends for the noise and Pearson’s correlation coefficient profiles. In proximity to the threshold, where all the free molecular species involved in the system are present in small numbers, both the noise measures we analyzed (Fano factor and coefficient of variation) show a maximum (for the latter coefficient the maximum is local). These behaviors are interpretable in terms of bimodal distributions for each molecular species involved in the titrative mechanism [33]. Interestingly the bimodality has been experimentally measured in a simple sRNA-mediated circuit in Bacteria [32], and could be potentially verified in our ceRNA case.

In proximity to such threshold value, also the Pearson’s correlation coefficients among ceRNAs or miRNAs show a maximum, meaning that the statistical correlation among molecules deriving from different genes is high. That is, not only the system is hypersensitive to little changes in the control parameter, but also fluctuations are highly correlated. As a matter of fact, the titration mechanism of interaction establishes a positive coupling among ceRNAs belonging to different genes (or among miRNAs). While the intensity of such correlation depends mostly on the combination the basal transcription rates of each particular gene (so that different genes speak each other at different intensities, but the level of correlation is established by the particular parameters), the location of the maximum is a determined by all the molecular species in competition. Furthermore, such statistical correlation is robust with respect to the number of ceRNAs involved in the system (with just a shift in the location of the threshold when increasing the number of ceRNAs) and also with respect to the catalyticity parameter α . When α is zero, meaning that all the miRNAs are recycled, it is still possible to observe the threshold effect and the maximum in correlations’ profiles as an out-of-equilibrium characteristic of the system. Thus, the *ceRNA effect* is always present, provided that the observation’s time is short enough.

To investigate experimentally these features, quantitative fluorescence microscopy seems, for the time being, the most promising technique. Previous works not directly related to the *ceRNA hypothesis* (see [10] for a seminal work in bacteria, and [16] in human cell lines) used two-colors fluorescent reporter systems. The construct typically consists of a bidirectional drug-inducible promoter driving the expression of the two fluorescent proteins. The 3’UTR of the fluorescent proteins can be engineered to control the binding sites, and so the miRNA-mRNA binding affinity for the targeting miRNAs of interest. Both in [10] and [16], the method was used to monitor the threshold effect in a simple sRNA/miRNA \rightarrow mRNA interaction. At the expenses of creating more complex constructs, an analogous technique could be deployed to investigate threshold, cross-talk, and noise/correlation behavior of simple ceRNA networks. In the most straightforward implementation one needs two reporter constructs: (i) the first construct consists of a bidirectional reporter system composed by the 3’UTR of ceRNA1 concatenated to the fluorescent gene (say green), and on the other side a miRNA binding site free 3’UTR concatenated to a second fluorescent gene (say yellow) to monitor the transcription activity, (ii) the second construct consists of a single reporter composed by the 3’UTR of ceRNA2 concatenated with a third fluorescent gene (say cherry). In this way one could simultaneously monitor the activity of both ceRNAs (green, cherry) as a function of the transcriptional activity of ceRNA1 (yellow) which would validate both qualitatively (in

terms of the profile predicted by the model) and possibly quantitatively (by allowing a multi-parametric fit of the model's kinetic constants from the experimental data) the model predictions as displayed, for instance, in Figure 2.

Finally, the model shows interesting out-of-equilibrium features around threshold which could be experimentally testable. In particular the peculiar response time profile as a function of the distance from the threshold could be directly measured by means of quantitative time-lapse fluorescence microscopy [35] and flow cytometry to monitor ceRNAs dynamics. To monitor the dynamics of two ceRNAs, one could conservatively construct a two colors fluorescent reporter system that allows for simultaneous monitoring of protein levels (see again [10, 16]). Of course larger networks could be potentially monitored using multiple colors.

Materials and Methods

Stochastic simulations

Stochastic simulations have been performed via implementation of Gillespie's first reaction algorithm [36].

Theoretical framework: stochastic model

In analogy with Figure 1B, for each gene belonging to the miRNA-target network in Figure 1A we consider the key steps of transcription, degradation and titrative interaction among transcripts. Thus, the system is described by $M + N$ variables (M miRNAs S_i and N target mRNAs R_j transcribed from $M + N$ different genes) and the probability of finding in a cell exactly $\mathbf{R}, \mathbf{S} := S_1, \dots, S_M, R_1, \dots, R_N$ molecules at time t satisfies the following master equation:

$$\begin{aligned} \partial_t P &= \sum_{i=1}^M k_{S_i} (P_{S_i-1} - P) + \sum_{j=1}^N k_{R_j} (P_{R_j-1} - P) + \\ &+ \sum_{i=1}^M g_{S_i} ((S_i + 1)P_{S_i+1} - S_i P) + \sum_{j=1}^N g_{R_j} ((R_j + 1)P_{R_j+1} - R_j P) + \\ &+ \alpha \sum_{i=1}^M \sum_{j=1}^N g_{ij} ((S_i + 1)(R_j + 1)P_{S_i+1, R_j+1} - S_i R_j P) + \\ &+ (1 - \alpha) \sum_{i=1}^M \sum_{j=1}^N g_{ij} S_i ((R_j + 1)P_{R_j+1} - R_j P), \end{aligned} \quad (1)$$

with $P = P_{X_1, \dots, X_k, \dots, X_{M+N}}$ and $P_{X_k \pm 1} = P_{X_1, \dots, X_k \pm 1, \dots, X_{M+N}}$. In Equation 1 k_{S_i} and k_{R_j} are transcription rates and g_{S_i} and g_{R_j} degradation rates for the i -th miRNA and the j -th target mRNA respectively. g_{ij} is the effective association rate for miRNA S_i and its target R_j . α is the catalyticity parameter described above.

By defining the generating function,

$$F(\mathbf{z}, \mathbf{q}|t) = \sum_{\mathbf{S}, \mathbf{R}} \prod_{i=1}^M \prod_{j=1}^N z_i^{S_i} q_j^{R_j} P_{\mathbf{R}, \mathbf{S}}, \quad (2)$$

where $\mathbf{z}, \mathbf{q} := z_1, \dots, z_M, q_1, \dots, q_N$, we can convert Equation 1 into the following second-order partial differential equation:

$$\partial_t F(\mathbf{z}, \mathbf{q}|t) = \mathcal{H}(\mathbf{z}, \mathbf{q}) F(\mathbf{z}, \mathbf{q}|t) \quad (3)$$

where the operator $\mathcal{H}(\mathbf{z}, \mathbf{q})$ is defined as:

$$\begin{aligned} \mathcal{H}(\mathbf{z}, \mathbf{q}) = & \sum_{i=1}^M k_{S_i}(z_i - 1) + \sum_{j=1}^N k_{R_j}(q_j - 1) + \\ & + \sum_{i=1}^M g_{S_i}(\partial_{z_i} - z_i \partial_{z_i}) + \sum_{j=1}^N g_{R_j}(\partial_{q_j} - q_j \partial_{q_j}) + \\ & + \alpha \sum_{i=1}^M \sum_{j=1}^N g_{ij}(\partial_{z_i, q_j}^2 - z_i q_j \partial_{z_i, q_j}^2) + (1 - \alpha) \sum_{i=1}^M \sum_{j=1}^N g_{ij} z_i (\partial_{z_i, q_j}^2 - q_j \partial_{z_i, q_j}^2). \end{aligned} \quad (4)$$

The moment generating function has the following properties:

$$\begin{aligned} F(\mathbf{z} = \mathbf{1}, \mathbf{q} = \mathbf{1}) &= 1, \\ \partial_{z_i} F|_{\mathbf{z}=\mathbf{1}, \mathbf{q}=\mathbf{1}} &= \langle S_i \rangle, \\ \partial_{q_j} F|_{\mathbf{z}=\mathbf{1}, \mathbf{q}=\mathbf{1}} &= \langle R_j \rangle, \\ \partial_{z_i}^2 F|_{\mathbf{z}=\mathbf{1}, \mathbf{q}=\mathbf{1}} &= \langle S_i^2 \rangle - \langle S_i \rangle, \\ \partial_{q_j}^2 F|_{\mathbf{z}=\mathbf{1}, \mathbf{q}=\mathbf{1}} &= \langle R_j^2 \rangle - \langle R_j \rangle, \\ \partial_{z_i, q_j}^2 F|_{\mathbf{z}=\mathbf{1}, \mathbf{q}=\mathbf{1}} &= \langle S_i R_j \rangle. \end{aligned} \quad (5)$$

Considering higher order derivatives in Equation 3 at steady state ($\partial_t F = 0$), and assuming that all derivatives are computed in $\mathbf{z} = \mathbf{1}, \mathbf{q} = \mathbf{1}$, we find:

$$\begin{aligned} \langle S_i \rangle &= \partial_{z_i} F = \frac{k_{S_i} - \alpha \sum_{j=1}^N g_{ij} \partial_{z_i, q_j}^2 F}{g_{S_i}}, \\ \langle R_j \rangle &= \partial_{q_j} F = \frac{k_{R_j} - \sum_{i=1}^M g_{ij} \partial_{z_i, q_j}^2 F}{g_{R_j}}, \\ \langle S_i^2 \rangle &= \partial_{z_i}^2 F + \partial_{z_i} F = \frac{k_{S_i}(1 + \partial_{z_i} F) - \alpha \sum_{j=1}^N g_{ij}(\partial_{z_i, q_j}^3 F + \partial_{z_i, q_j}^2 F)}{g_{S_i}}, \\ \langle R_j^2 \rangle &= \partial_{q_j}^2 F + \partial_{q_j} F = \frac{k_{R_j}(1 + \partial_{q_j} F) - \sum_{i=1}^M g_{ij}(\partial_{z_i, q_j}^3 F + \partial_{z_i, q_j}^2 F)}{g_{R_j}}, \\ \langle S_i R_j \rangle &= \frac{k_{R_j} \partial_{z_i} F + k_{S_i} \partial_{q_j} F - \sum_{l=1}^M g_{lj} \partial_{z_i, z_l, q_j}^3 F - \alpha \sum_{l=1}^N g_{il} \partial_{z_i, q_j, q_l}^3 F}{g_{ij} + g_{S_i} + g_{R_j}}, \\ &\text{etc...} \end{aligned} \quad (7)$$

The moment-generating function defined in Equation 3 is unfortunately too complicated to be computed analytically even at steady state, as all moments depend on higher ones and the system is not closed, as shown in Equation 7. In the following we will present a series of increasingly accurate approximations for analyzing it.

Independent molecular-species approximation

As a first step for determining analytically the behavior of the system, we will assume that the probability distribution P is factorized:

$$P^{\text{ind}}(\mathbf{R}, \mathbf{S}) := \prod_{i=1}^M P_i^S(S_i) \prod_{j=1}^N P_j^R(R_j) \quad (8)$$

Under this assumption it turns out that the steady state solution for the $P_i^S(S_i)$, and $P_j^R(R_j)$ are Poisson distributions whose mean value can be expressed solving the following second order system of equations,

$$\begin{aligned} \langle S_i \rangle_{\text{ind}} &= \frac{k_{S_i} - \alpha \langle S_i \rangle_{\text{ind}} \sum_{j=1}^N g_{ij} \langle R_j \rangle_{\text{ind}}}{g_{S_i}} \quad 1 \leq i \leq M \\ \langle R_j \rangle_{\text{ind}} &= \frac{k_{R_j} - \langle R_j \rangle_{\text{ind}} \sum_{i=1}^M g_{ij} \langle S_i \rangle_{\text{ind}}}{g_{R_j}} \quad 1 \leq j \leq N. \end{aligned} \quad (9)$$

Analytic solutions for the system of equations 10 can be easily written in the case $g_{R_j} = g_R$, $g_{S_i} = g_S$ and $g_{ij} = g$ for all R_j and S_i :

$$\begin{aligned} \langle S_q \rangle_{\text{ind}} &= \frac{k_{S_q}}{2g_S \sum_{i=1}^M k_{S_i}} \left(k_{S_q} + \sum_{i \neq q}^M k_{S_i} - \alpha \sum_{j=1}^N k_{R_j} - \frac{g_R g_S - \sqrt{A}}{g} \right) \\ \langle R_p \rangle_{\text{ind}} &= \frac{k_{R_p}}{2g_R \sum_{j=1}^N k_{R_j}} \left(k_{R_p} + \sum_{j \neq p}^N k_{R_j} - \sum_{i=1}^M k_{S_i} - \frac{g_R g_S - \sqrt{A}}{\alpha g} \right), \end{aligned} \quad (10)$$

with $A = 4gg_S g_R \alpha \sum_{j=1}^N k_{R_j} + (g_R g_S + g(\sum_{i=1}^M k_{S_i} - \alpha \sum_{j=1}^N k_{R_j}))^2$. In the more general and biologically relevant case of different molecules half-lives and complex affinities g_{ij} , solutions can still be found, but they turn out to be too complex and long to be reported here.

Locating the threshold

The simplest way to locate the threshold is to solve the system of equations 10 in the limit of strong interaction miRNA-target (high g_{ij}) thus finding:

$$\begin{aligned} \langle S_i \rangle_{\text{ind,ss}} &\rightarrow \begin{cases} \frac{k_{S_i} - \alpha \sum_{j=1}^N k_{R_j}}{g_{S_i}} & \text{if } \alpha \sum_{j=1}^N k_{R_j} < \sum_{i=1}^M k_{S_i} \\ 0 & \text{otherwise} \end{cases} \\ \langle R_j \rangle_{\text{ind,ss}} &\rightarrow \begin{cases} \frac{k_{R_j} - \sum_{i=1}^M k_{R_j} k_{S_i} / (\alpha \sum_{j=1}^N k_{R_j})}{g_{R_j}} & \text{if } \alpha \sum_{j=1}^N k_{R_j} \geq \sum_{i=1}^M k_{S_i} \\ 0 & \text{otherwise} \end{cases} \end{aligned} \quad (11)$$

The threshold position is determined by the relative amount of miRNAs and their targets (see Equation 11). For fixed k_{R_j} and k_{S_i} , with $j = \{1, \dots, q-1, q+1, \dots, N\}$ and $i = \{1, \dots, M\}$, the threshold is set by k_{R_q} and by all miRNA transcription rates k_{S_i} . Thus, as long as the q-th mRNA target transcription rate k_{R_q} is below its threshold level $k_{R_q}^* = (\sum_{i=1}^M k_{S_i} - \alpha \sum_{j \neq q}^N k_{R_j}) / \alpha$ all targets are bound in complexes and their free molecule amount is very low (while miRNAs are expressed), or, in other terms, the threshold is located at near-equimolar concentration of the different chemical species.

Increasing k_{R_q} beyond its threshold results in the expression of all the other targets (while miRNAs will be all bound in complexes), see Figure 2A.

Within the independent chemical species approximation in Equation 8 the Fano factor (noise index $f\langle X \rangle = \sigma_{\langle X \rangle}^2 / \langle X \rangle$) for each molecular species is 1. The factorized approximation is good enough in showing the threshold effect, but fails in determining correlations among molecular species (see symbols, which are the results of Gillespie’s simulations, in Figures 2A and 3A).

Gaussian Approximation

The simplest approximation beyond mean-field is a Gaussian one. We denote $\vec{X} = (X_1, \dots, X_{N+M}) := (R_1, \dots, R_N, S_1, \dots, S_M)$. The approximation assumes that \vec{X} is distributed as a multivariate Gauss:

$$P(\vec{X}) = \frac{\exp \left[-\frac{1}{2} (\vec{X} - \vec{\mu})^T C^{-1} (\vec{X} - \vec{\mu}) \right]}{\sqrt{(2\pi)^{N+M} \det(C)}} \quad , \quad (12)$$

where the covariance matrix C has coordinates $c_{ij} := E(X_i X_j) - E(X_i)E(X_j)$, the vector $\vec{\mu}$ has coordinates $\mu_i := E(X_i)$, and the expectation value $E(\cdot)$ is with respect to the Gaussian measure P defined in Equation 12. All moments of a Gaussian multivariate measure can be expressed in terms of μ_i and c_{ij} . Therefore the moments derived from the generating function in Equation 7 can be expressed in terms of μ_i and c_{ij} . In the Supplementary Material we describe in details the computation of the specific $N = M = 2$ case, and we compare the performance of the Gaussian approximation with the linear-noise approximation.

Acknowledgments

While completing this manuscript we learned that M. Figliuzzi, E. Marinari, and A. De Martino have independently studied the same problem, reporting results which are consistent with those obtained here.

We thank Michele Caselle, Enzo Marinari, Paolo Provero, Andrea De Martino, Luca Dall’Asta, Carlo Baldassi, Matteo Osella, Marco Zamparo, and Matteo Figliuzzi, for interesting discussions about technical aspects of stochastic modeling. We are indebted with Pier Paolo Pandolfi, Yvonne Tay, Florian Karreth, and Riccardo Taulli for many illuminating discussions about the experimental strategies for validating the model, and Terence Hwa for pointing us a relevant bibliographic reference on the subject. RZ acknowledges support from the ERC Grant No. OPTINF 267915.

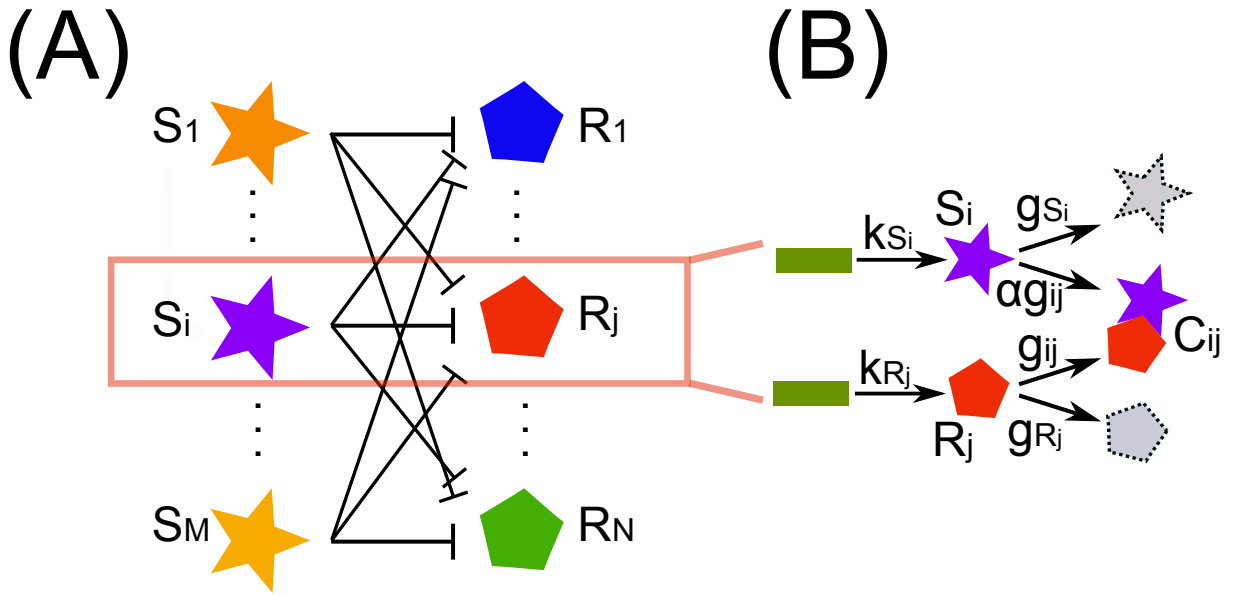


Figure 1. Representation of a generic miRNA-target interaction network. (A) Simplified picture of a miRNA-ceRNA interaction network. (B) For each miRNA (S_i) and ceRNA (R_j) present in the network we consider the main steps of transcription (rates k_{S_i} and k_{R_j} respectively) and degradation (rates g_{S_i} and g_{R_j} respectively) plus a titrative interaction between miRNA and ceRNA. miRNA and ceRNA can therefore form a complex C_{ij} with effective association rate g_{ij} . The parameter α (the catalyticity parameter) tells which is the probability a miRNA is recycled after having interact with one of its targets.

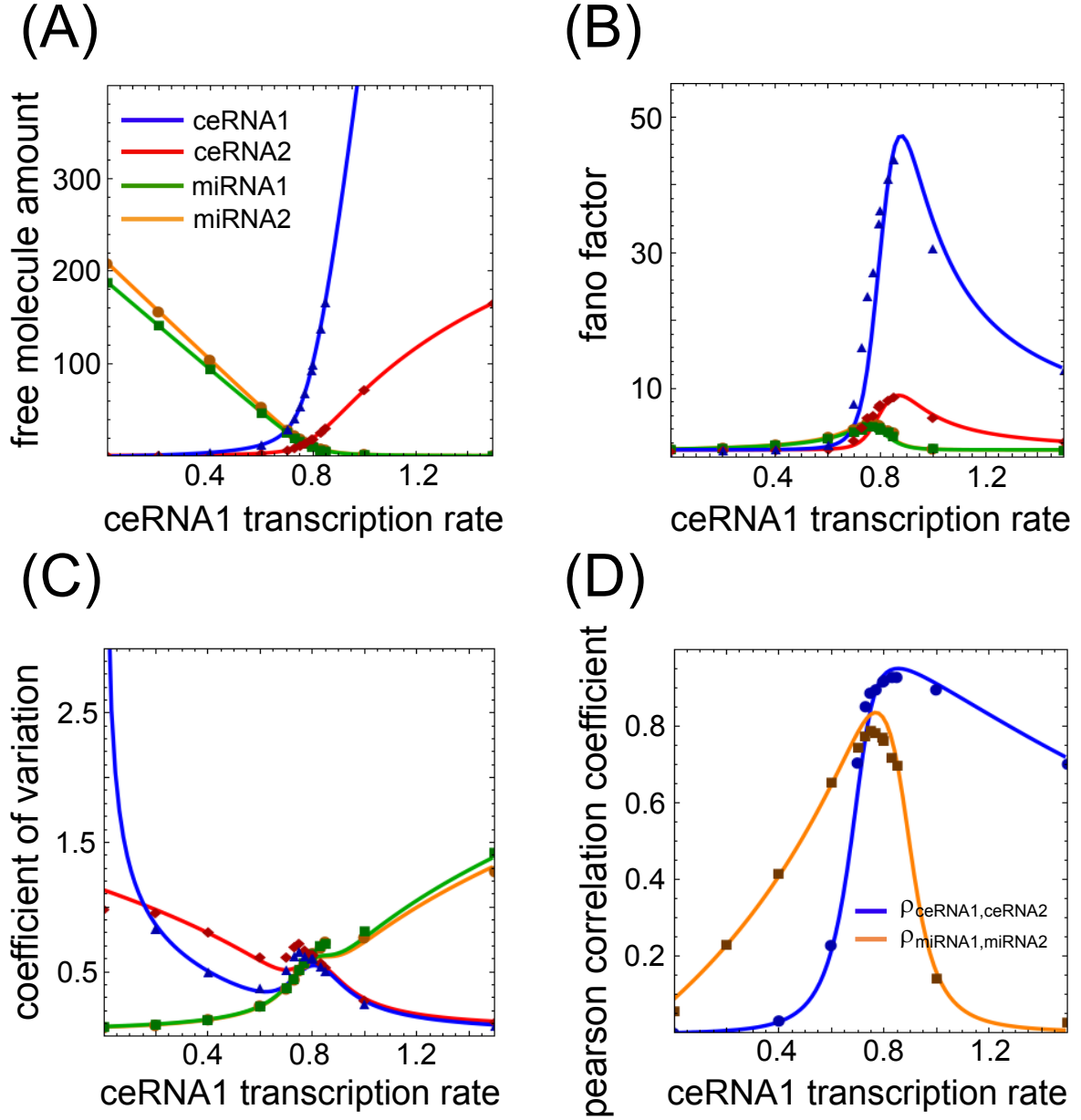


Figure 2. *Threshold, noise and Pearson's correlation coefficient varying ceRNA transcription rate.* (A-C) Steady state value for means, Fano factors and coefficients of variation for each free molecular species in a system of two miRNAs (miRNA1 and miRNA2, green and orange lines respectively) interacting with two ceRNAs (ceRNA1 and ceRNA2, blue and red lines respectively) varying the concentration of ceRNA1. In proximity to the threshold the system shows hypersensitivity to changes in the control parameter (ceRNA1 transcription rate), captured by a maximum in the Fano factors (panel B). For the same values of ceRNA1 transcription rate, the local maximum in the coefficients of variation (panel C) is the fingerprint of bimodal distributions in the number of molecules for each molecular species. (D) Pearson's coefficients between the two miRNAs (orange line) and the two ceRNAs (blue line). The two lines show a maximum in proximity to the ceRNA1 transcription rate threshold value, meaning that there is a region of parameters where the fluctuations in the number of ceRNAs or miRNAs are highly correlated. Lines are the results of Gaussian approximation while symbols are Gillespie's simulations. For panels B,C the line color-code is the same as in panel A.

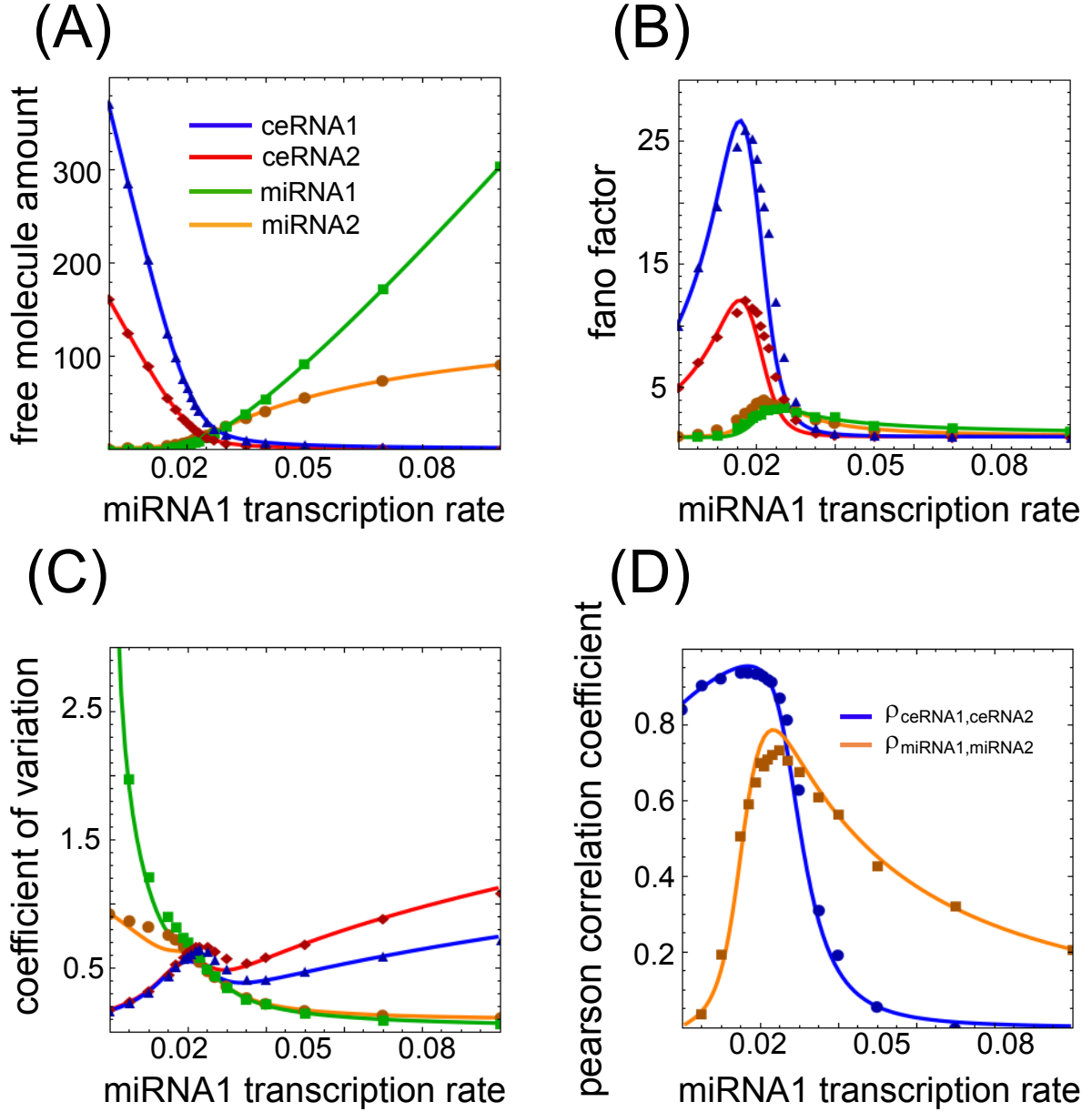


Figure 3. *Threshold, noise and Pearson's correlation coefficient varying miRNA transcription rate.* (A-C) Steady state value for means, Fano factors and coefficients of variation for each free molecular species in a system of two miRNAs (miRNA1 and miRNA2, green and orange lines respectively) interacting with two ceRNAs (ceRNA1 and ceRNA2, blue and red lines respectively) varying the concentration of miRNA1. In proximity to the threshold the system shows hypersensitivity to changes in the control parameter (miRNA1 transcription rate), captured by a maximum in the Fano factors (panel B). For the same values of miRNA1 transcription rate, the local maximum in the coefficients of variation (panel C) is the fingerprint of bimodal distributions in the number of molecules for each molecular species. (D) Pearson's coefficients between the two miRNAs (orange line) and the two ceRNAs (blue line). The two lines show a maximum in proximity to the miRNA1 transcription rate threshold value, meaning that there is a region of parameters where the fluctuations in the number of ceRNAs or miRNAs are highly correlated. Lines are the results of Gaussian approximation while symbols are Gillespie's simulations. For panels B,C the line color-code is the same as in panel A.

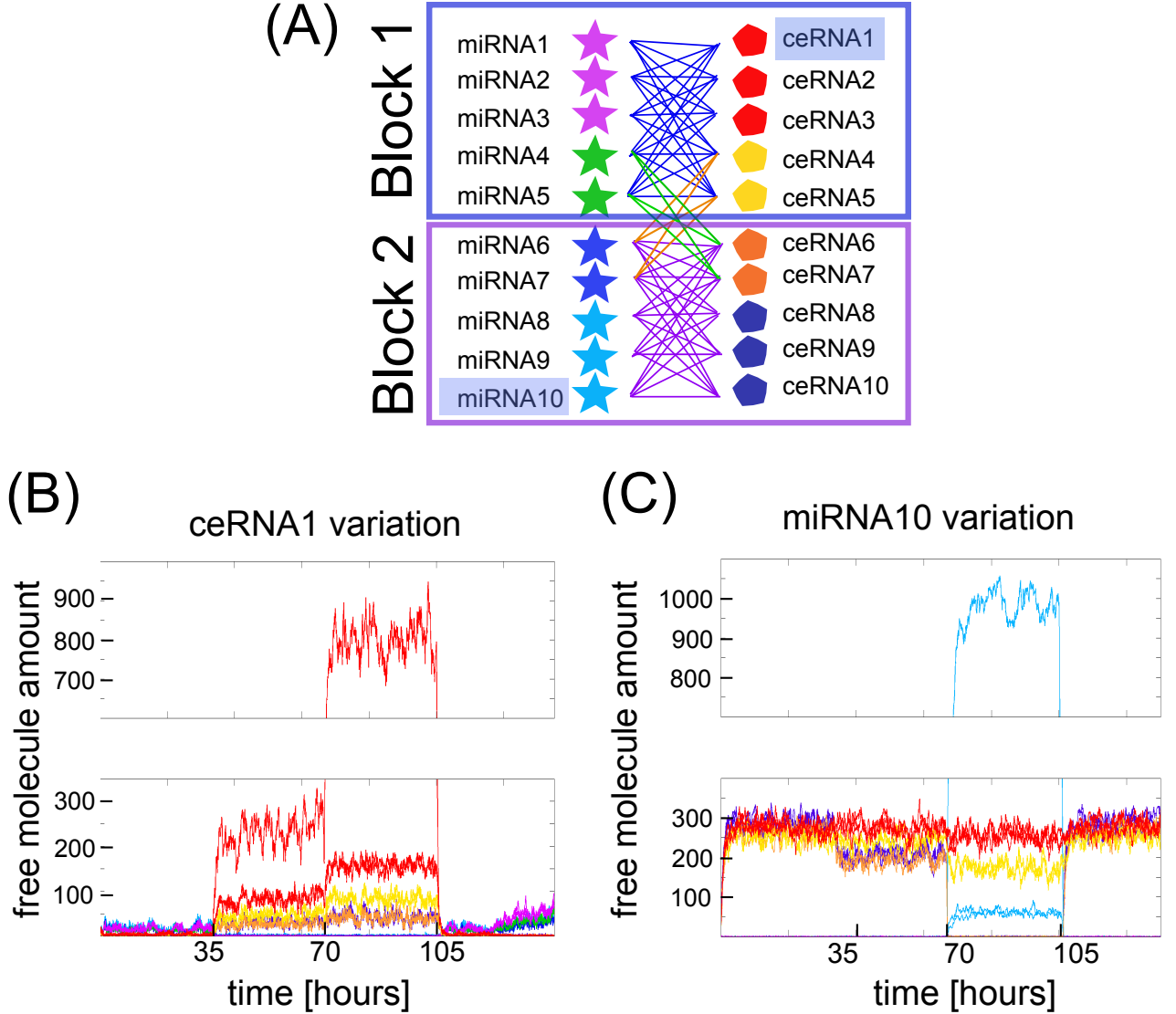


Figure 4. *Selectivity of miRNA and ceRNA interactions.* (A) Example of a network of ten miRNAs interacting with ten ceRNAs in blocks. The interaction links are such that we can define two main blocks (block 1 and block2) of strongly interacting miRNAs-ceRNAs connected by two common miRNAs (miRNA 4 and 5 in block 1, miRNA 6 and 7 in block 2) and ceRNAs (ceRNA 4 and 5 in block 1 and ceRNA 6 and 7 in block 2). Panels (B,C) show an example of dynamics of such network. Varying ceRNA1 (panel B) or miRNA10 (panel C) transcription rate during time (every 35 hours in the example, but the time is arbitrary) has a differentiated effect on the other ceRNAs and miRNAs present in the all network. The color-code for lines in panels B and C follows the color of miRNAs and ceRNAs in panel A.

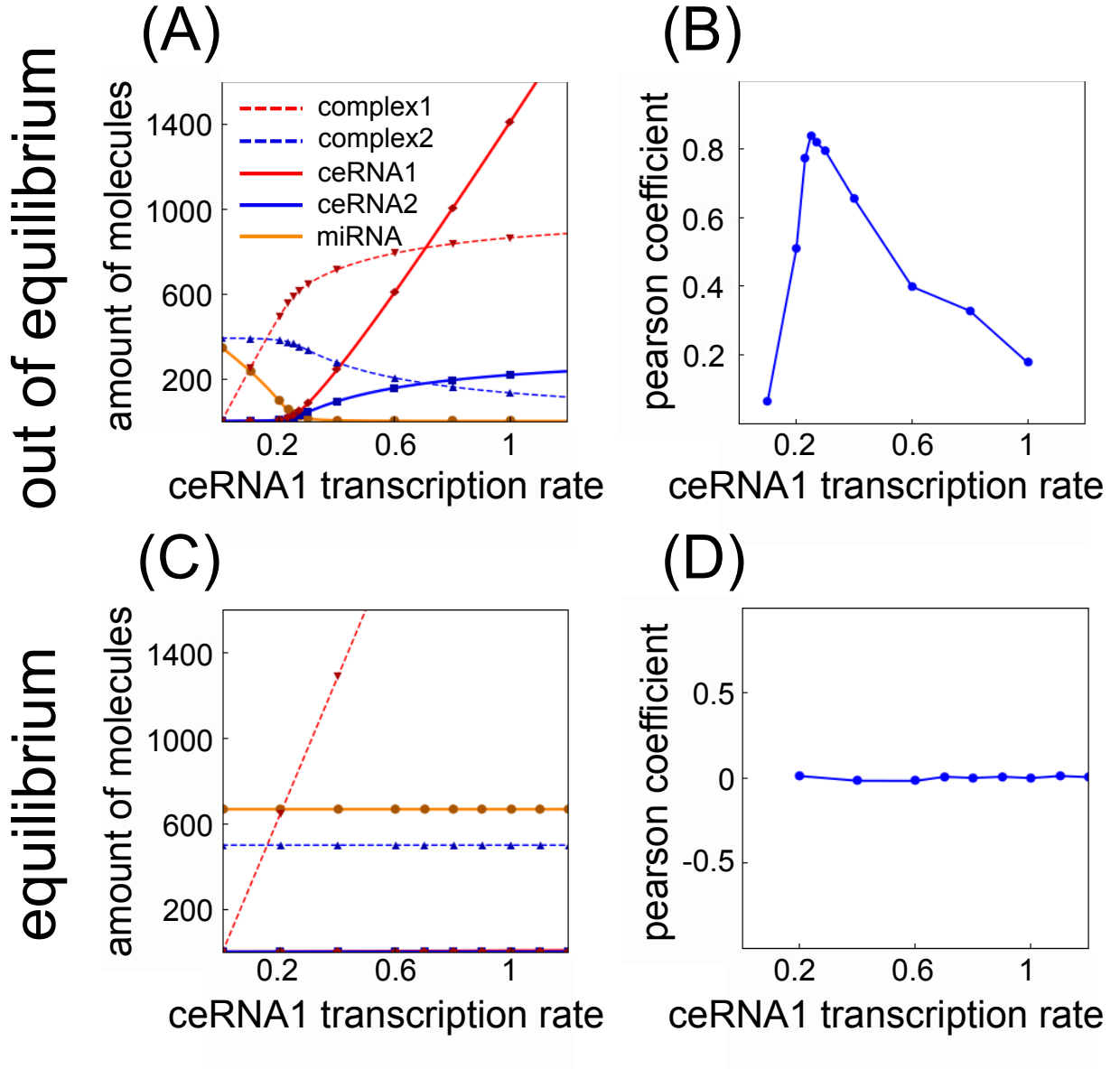


Figure 5. *Threshold effect in a miRNA-target catalytic interaction.* Example of a system of one miRNA interacting with two ceRNAs with cataliticity parameter $\alpha = 0$. The threshold effect is possible only if the system is out of equilibrium (A). Numerical integration of Equation (1) in Supplementary Materials leads to time evolution of each molecular species for a given set of parameters. In panels A,C we plot “pictures” of the evolving system at different time t (panel A $t = 10^3$, panel C $t = 10^6$) as a function of ceRNA1 transcription rate. When t is smaller than the time complexes need to reach their steady state a threshold effect is observed. In panels B,D we plot the corresponding Pearson’s coefficient profiles. Where the threshold effect is present (panel A), a peak in the Pearson’s coefficient is also observed.

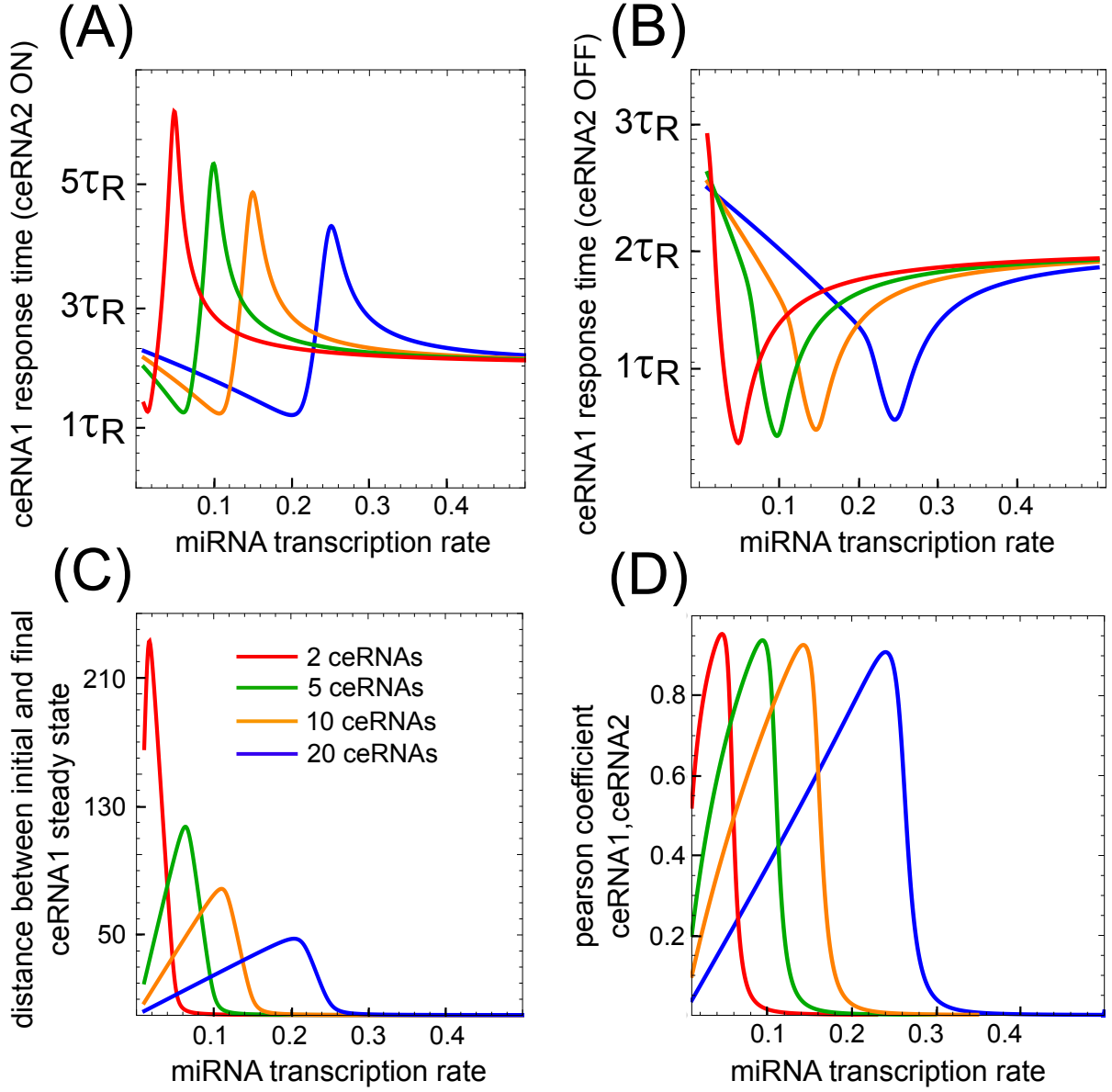


Figure 6. *Response times upon one ceRNA perturbation.* Increasing miRNA transcription rate ceRNA1 shows a maximum and a minimum in its response times upon switching on or off ceRNA2 transcription respectively (panel A and B). The maximum (minimum) is located near the threshold, where ceRNA1 initial value (that is its values before switching on (off) ceRNA2) is near to the steady state it will reach upon switching on (off) ceRNA2 (panel C) but also the more sensitive to ceRNA2 variation (look at the maximum in the Pearson's correlation coefficient between ceRNA1 and ceRNA2 in panel D). Different color lines correspond to different numbers of ceRNAs in competition for the same miRNA. The qualitative trend for response times and Pearson's correlation coefficient is robust with respect to increasing such number.

Supplementary Material

A Generalized mean-field equation with explicit complexes

We describe the general case of N different target mRNAs interacting with M different miRNAs. The action of a miRNA on its target has the following characteristics: each miRNA molecule can constitute a complex with a target molecule and then can be eventually released. The molecular species are: free miRNAs (S_i), free mRNAs (R_j), complexes C_{ij} of miRNA S_i with mRNA R_j . Each gene can be transcribed with rate $k_{\{R_i, S_j\}}$, degraded with rate $g_{\{R_i, S_j\}}$. Complexes C_{ij} associate with rate k_{ij}^+ and dissociate with rate k_{ij}^- . Each complex eventually degrades with rate γ_{ij} . A schema of such network is represented in Figure 7. The mean-field equations thus reads:

$$\begin{aligned}\frac{dR_i}{dt} &= k_{R_i} - g_{R_i}S_j + \sum_{j=1}^M (-k_{ij}^+ S_j R_i + k_{ij}^- C_{ij}) \\ \frac{dS_j}{dt} &= k_{S_j} - g_{S_j}S_j + \sum_{i=1}^N (-k_{ij}^+ S_i R_j + k_{ij}^- C_{ij} + (1 - \alpha)\gamma_{ij}C_{ij}) \\ \frac{dC_{ij}}{dt} &= k_{ij}^+ R_i S_j - (k_{ij}^- + \gamma_{ij})C_{ij}\end{aligned}\tag{13}$$

with $j \in \{i, \dots, M\}$ and $i \in \{1, \dots, N\}$. Assuming that complexes reach the equilibrium faster than the other molecular species, we can simplify the system 13 to the following one:

$$\begin{aligned}\frac{dS_i}{dt} &= k_{S_i} - g_{S_i}S_i - \alpha g_{ij}S_i R_j \\ \frac{dR_j}{dt} &= k_{R_j} - g_{R_j}R_j - g_{ij}S_i R_j,\end{aligned}\tag{14}$$

with $g_{ij} = \frac{k_{ij}^+ \gamma_{ij}}{k_{ij}^- + \gamma_{ij}}$.

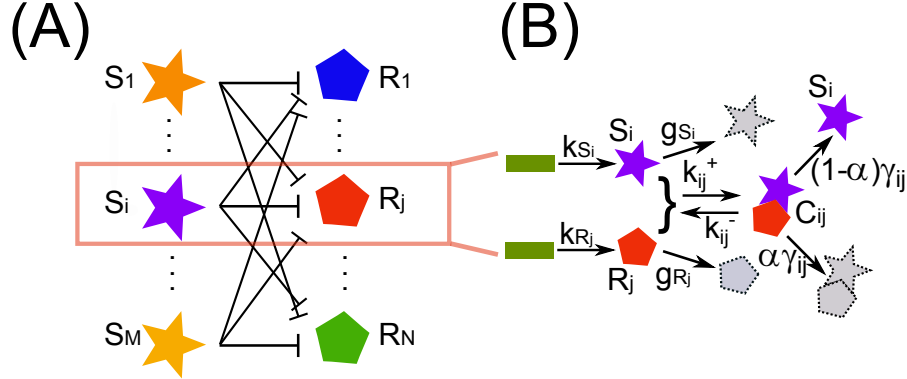


Figure 7. Representation of a generic miRNA-target interaction network. (A) Simplified picture of a miRNA-ceRNA interaction network. (B) For each miRNA (S_i) and ceRNA (R_j) present in the network we consider the main steps of transcription (rates k_{S_i} and k_{R_j} respectively) and degradation (rates g_{S_i} and g_{R_j} respectively) plus a titrative interaction between miRNA and ceRNA. miRNA and ceRNA can therefore form a complex C_{ij} with association rate k_{ij}^+ and dissociation rate k_{ij}^- . The complex can then degrade with rate γ_{ij} . The parameter α (the catalyticity parameter) tells which is the probability a miRNA is recycled after having interact with one of its targets.

B Generalized master equation with explicit complexes

The master equation corresponding to Equation 13 reads:

$$\begin{aligned}
 \partial_t P = & \sum_{i=1}^M k_{S_i} (P_{S_i-1, R_j, C_{ij}} - P_{S_i, R_j, C_{ij}}) + \sum_{j=1}^N k_{R_j} (P_{S_i, R_j-1, C_{ij}} - P_{S_i, R_j, C_{ij}}) + \\
 & + \sum_{i=1}^M g_{S_i} ((S_i + 1) P_{S_i+1, R_j, C_{ij}} - S_i P_{S_i, R_j, C_{ij}}) + \sum_{j=1}^N g_{R_j} ((R_j + 1) P_{S_i, R_j+1, C_{ij}} - R_j P_{S_i, R_j, C_{ij}}) + \\
 & + \sum_{i=1}^M \sum_{j=1}^N k_{ij}^+ ((S_i + 1)(R_j + 1) P_{S_i+1, R_j+1, C_{ij}-1} - S_i R_j P_{S_i, R_j, C_{ij}}) + \\
 & + \sum_{i=1}^M \sum_{j=1}^N k_{ij}^- ((C_{ij} + 1) P_{S_i-1, R_j-1, C_{ij}+1} - C_{ij} P_{S_i, R_j, C_{ij}}) + \\
 & + \alpha \sum_{i=1}^M \sum_{j=1}^N \gamma_{ij} ((C_{ij} + 1) P_{S_i, R_j, C_{ij}+1} - C_{ij} P_{S_i, R_j, C_{ij}}) + \\
 & + (1 - \alpha) \sum_{i=1}^M \sum_{j=1}^N \gamma_{ij} ((C_{ij} + 1) P_{S_i-1, R_j, C_{ij}+1} - C_{ij} P_{S_i, R_j, C_{ij}}),
 \end{aligned} \tag{15}$$

C Gaussian Approximation

We work here in some details the explicit computation for the Gaussian approximation in the specific case of 2 microRNAs (S_1, S_2) and 2 ceRNAs (R_1, R_2). Denoting with $\partial_{z_i^l, q_j^m}^{l+m} F := \partial_{z_i^l, q_j^m}^{l+m} F|_{\mathbf{z}, \mathbf{q}=(1, \dots, 1)}$, at

steady state the system of equation reads:

$$\begin{aligned}
\partial_{z_1} F &= \frac{k_{z_1} - \alpha g(\partial_{z_1, q_1}^2 F + \partial_{z_1, q_2}^2 F)}{g_S} \\
\partial_{z_2} F &= \frac{k_{z_2} - \alpha g(\partial_{z_2, q_1}^2 F + \partial_{z_2, q_2}^2 F)}{g_S} \\
\partial_{q_1} F &= \frac{k_{q_1} - g(\partial_{z_1, q_1}^2 F + \partial_{z_2, q_1}^2 F)}{g_R} \\
\partial_{q_2} F &= \frac{k_{q_2} - g(\partial_{z_1, q_2}^2 F + \partial_{z_2, q_2}^2 F)}{g_R} \\
\partial_{z_1}^2 F &= \frac{k_{z_1} \partial_{z_1} F - \alpha g(\partial_{z_1, q_1}^3 F + \partial_{z_1, q_2}^3 F)}{g_S} \\
\partial_{z_1, z_2}^2 F &= \frac{k_{z_2} \partial_{z_1} F + k_{z_1} \partial_{z_2} F - 2\alpha g(\partial_{z_1, z_2, q_1}^3 F + \partial_{z_1, z_2, q_2}^3 F)}{2g_S} \\
\partial_{z_1, q_1}^2 F &= \frac{k_{q_1} \partial_{z_1} F + k_{z_1} \partial_{q_1} F - g(\partial_{z_1, q_1}^3 F + \partial_{z_1, z_2, q_1}^3 F + \alpha \partial_{z_1, q_1^2}^3 F + \alpha \partial_{z_2, q_1, q_2}^3 F)}{g + g_R + g_S} \\
\partial_{z_1, q_2}^2 F &= \frac{k_{q_2} \partial_{z_1} F + k_{z_1} \partial_{q_2} F - g(\partial_{z_1, q_2}^3 F + \partial_{z_1, z_2, q_2}^3 F + \alpha \partial_{z_1, q_1, q_2}^3 F + \partial_{z_2, R_2}^3 F)}{g + g_R + g_S} \\
\partial_{z_2}^2 F &= \frac{k_{z_2} \partial_{z_2} F - \alpha g(\partial_{z_2, q_1}^3 F + \partial_{z_2, q_2}^3 F)}{g_S} \\
\partial_{z_2, q_1}^2 F &= \frac{k_{q_1} \partial_{z_2} F + k_{z_2} \partial_{q_1} F - g(\partial_{z_1, z_2, q_1}^3 F + \partial_{z_2, q_1}^3 F + \alpha \partial_{z_2, q_1^2}^3 F + \alpha \partial_{z_2, q_1, q_2}^3 F)}{g + g_R + g_S} \\
\partial_{z_2, q_2}^2 F &= \frac{k_{q_2} \partial_{z_2} F + k_{z_2} \partial_{q_2} F - g(\partial_{z_1, z_2, q_1}^3 F + \partial_{z_2, q_1}^3 F + \alpha \partial_{z_2, q_1^2}^3 F + \alpha \partial_{z_2, q_1, q_2}^3 F)}{g + g_R + g_S} \\
\partial_{q_1}^2 F &= \frac{k_{q_1} \partial_{q_1} F - g(\partial_{z_1, q_1^2}^3 F + \partial_{z_2, q_1}^3 F)}{g_R} \\
\partial_{q_1, q_2}^2 F &= \frac{k_{q_2} \partial_{q_1} F + k_{q_1} \partial_{q_2} F - 2g(\partial_{z_1, q_1, q_2}^3 F + \partial_{z_2, q_1, q_2}^3 F)}{g + g_R + g_S} \\
\partial_{q_2}^2 F &= \frac{k_{q_2} \partial_{q_2} F - g(\partial_{z_1, q_2^2}^3 F + \partial_{z_2, q_2}^3 F)}{g_R}
\end{aligned} \tag{16}$$

Recalling that within the Gaussian approximation the partial derivatives of the third order can be

expressed in terms of that of lower order:

$$\begin{aligned}
\partial_{z_1, z_2}^3 F &= (\partial_{z_1}^2 F + \partial_{z_1} F) \partial_{z_2} F + 2 \partial_{z_1} F \partial_{z_1, z_2}^2 F - 2 (\partial_{z_1} F)^2 \partial_{z_2} F - \partial_{z_1, z_2}^2 F \\
\partial_{z_1, q_1}^3 F &= (\partial_{z_1}^2 F + \partial_{z_1} F) \partial_{q_1} F + 2 \partial_{z_1} F \partial_{z_1, q_1}^2 F - 2 (\partial_{z_1} F)^2 \partial_{q_1} F - \partial_{z_1, q_1}^2 F \\
\partial_{z_1, q_2}^3 F &= (\partial_{z_1}^2 F + \partial_{z_1} F) \partial_{q_2} F + 2 \partial_{z_1} F \partial_{z_1, q_2}^2 F - 2 (\partial_{z_1} F)^2 \partial_{q_2} F - \partial_{z_1, q_2}^2 F \\
\partial_{z_1, z_2}^3 F &= (\partial_{z_2}^2 F + \partial_{z_2} F) \partial_{z_1} F + 2 \partial_{z_2} F \partial_{z_1, z_2}^2 F - 2 (\partial_{z_2} F)^2 \partial_{z_1} F - \partial_{z_1, z_2}^2 F \\
\partial_{z_1, q_1}^3 F &= (\partial_{q_1}^2 F + \partial_{q_1} F) \partial_{z_1} F + 2 \partial_{q_1} F \partial_{z_1, q_1}^2 F - 2 (\partial_{q_1} F)^2 \partial_{z_1} F - \partial_{z_1, q_1}^2 F \\
\partial_{z_1, q_2}^3 F &= (\partial_{q_2}^2 F + \partial_{q_2} F) \partial_{z_1} F + 2 \partial_{q_2} F \partial_{z_1, q_2}^2 F - 2 (\partial_{q_2} F)^2 \partial_{z_1} F - \partial_{z_1, q_2}^2 F \\
\partial_{z_2, q_1}^3 F &= (\partial_{z_2}^2 F + \partial_{z_2} F) \partial_{q_1} F + 2 \partial_{z_2} F \partial_{z_2, q_1}^2 F - 2 (\partial_{z_2} F)^2 \partial_{q_1} F - \partial_{z_2, q_1}^2 F \\
\partial_{z_2, q_2}^3 F &= (\partial_{z_2}^2 F + \partial_{z_2} F) \partial_{q_2} F + 2 \partial_{z_2} F \partial_{z_2, q_2}^2 F - 2 (\partial_{z_2} F)^2 \partial_{q_2} F - \partial_{z_2, q_2}^2 F \\
\partial_{z_2, q_1}^3 F &= (\partial_{q_1}^2 F + \partial_{q_1} F) \partial_{z_2} F + 2 \partial_{q_1} F \partial_{z_2, q_1}^2 F - 2 (\partial_{q_1} F)^2 \partial_{z_2} F - \partial_{z_2, q_1}^2 F \\
\partial_{z_2, q_2}^3 F &= (\partial_{q_2}^2 F + \partial_{q_2} F) \partial_{z_2} F + 2 \partial_{q_2} F \partial_{z_2, q_2}^2 F - 2 (\partial_{q_2} F)^2 \partial_{z_2} F - \partial_{z_2, q_2}^2 F \\
\partial_{z_1, z_2, q_1}^3 F &= \partial_{z_1, z_2}^2 \partial_{q_1} F + \partial_{z_2, q_1}^2 \partial_{z_1} F + \partial_{z_1, q_1}^2 \partial_{z_2} F - 2 \partial_{z_1} F \partial_{z_2} F \partial_{q_1} F \\
\partial_{z_1, z_2, q_2}^3 F &= \partial_{z_1, z_2}^2 \partial_{q_2} F + \partial_{z_2, q_2}^2 \partial_{z_1} F + \partial_{z_1, q_2}^2 \partial_{z_2} F - 2 \partial_{z_1} F \partial_{z_2} F \partial_{q_2} F \\
\partial_{z_2, q_1, q_2}^3 F &= \partial_{z_2, q_1}^2 \partial_{q_2} F + \partial_{z_2, q_2}^2 \partial_{q_1} F + \partial_{q_1, q_2}^2 \partial_{z_2} F - 2 \partial_{z_2} F \partial_{q_1} F \partial_{q_2} F \\
\partial_{z_1, q_1, q_2}^3 F &= \partial_{z_1, q_1}^2 \partial_{q_2} F + \partial_{z_1, q_2}^2 \partial_{q_1} F + \partial_{q_1, q_2}^2 \partial_{z_1} F - 2 \partial_{z_1} F \partial_{q_1} F \partial_{q_2} F
\end{aligned} \tag{17}$$

Inserting relations (17) into (16) we obtain a closed system of 14 in 14 unknowns. In the general case of a network of N ceRNAs interacting through M miRNAs we would have a complete system of $2(N + M) + \binom{N+M}{2}$ equations.

D Linear noise approximation

We use the linear noise approximation [30] in order to obtain the steady state fluctuation covariance matrix directly from the macroscopic system. For a general system of M miRNAs interacting with N mRNAs and R elementary reactions, we assign to each reaction r a propensity f_r defined from the probability $\Omega f_r(\psi, \Omega) \delta t$ that a reaction r occurs in the homogeneous system volume Ω in the time interval δt . ψ is the concentration vector of the $M + N$ chemical components of the system. In the macroscopic limit ($\Omega \rightarrow \infty$) the system dynamics is described by the following $M + N$ ordinary differential equations,

$$\frac{d\psi_p}{dt} = \sum_r \nu_{rp} f_r(\psi_1, \dots, \psi_{M+N}), \tag{18}$$

where ν_{rp} is the rp -th element of the stoichiometry matrix, i.e. it indicates the number of molecules by which a component p changes when an elementary reaction of type r occurs.

For small enough deviations $\delta\psi = [\delta\psi_1, \delta\psi_2, \dots, \delta\psi_{M+N}]$ from its steady state, the dynamics of Equation (18) can be approximated by a system of linear differential equations, according to $\frac{\delta\psi}{dt} = \mathcal{A} \delta\psi$, where \mathcal{A} is the Jacobian matrix with elements

$$a_{pq} = \sum_{r=1}^R \nu_{rp} \left(\frac{\partial f_r}{\partial \psi_q} \right)_{\psi_{ss}}. \tag{19}$$

The master equation for the probability of having $X = [X_1, X_2, \dots, X_p, \dots, X_{M+N}]$ molecules in the

system at time t is then

$$\frac{dP}{dt}(X, t) = \Omega \sum_{r=1}^R \left(\prod_{p=1}^N E_p^{\nu_{rp}} - 1 \right) f_r(X \Omega^{-1}, \Omega) P(X, t), \quad (20)$$

with E being a step operator with property $E_p^{\nu_{rp}} g(\dots, X_p, \dots) = g(\dots, X_p + \nu_{rp}, \dots)$.

To obtain the linear noise approximation [30] we expand the master equation to second order in $\Omega^{-1/2}$ after substituting each p -th component of X with $X_p = \Omega \psi_p + \Omega^{1/2} x_p$. x_p is the p -th component of a new random vector x such that the X_p is thus described as a macroscopic term $\Omega \psi_p$ plus a stochastic term $\Omega^{1/2} x_p$. We thus obtain a linear Fokker-Planck equation for the joint probability distribution $\Pi(x, t)$ of x :

$$\frac{d\Pi}{dt}(x, t) = - \sum_{p,q} a_{pq} \frac{\partial x_p \Pi}{\partial x_p} + \frac{1}{2} \sum_{p,q} b_{pq} \frac{\partial^2 \Pi}{\partial x_p \partial x_q}. \quad (21)$$

The matrix elements a_{pq} are given by the Jacobian matrix \mathcal{A} , while the elements b_{pq} of the diffusion matrix \mathcal{B} are defined as in [37],

$$b_{pq} = \sum_{r=1}^R f_r \nu_{rp} \nu_{rq}. \quad (22)$$

Generally \mathcal{A} and \mathcal{B} may depend on time, but here we will restrict our analysis to the steady state case. In this way, the stationary solution of Equation (21) is the normal distribution $N(0, \Xi)$. Ξ , which is the covariance matrix with elements ξ_{rp} , is the solution of the matrix Lyapunov equation:

$$\mathcal{A}\Xi + \Xi\mathcal{A}^T + \mathcal{B} = 0 \quad (23)$$

The covariance matrix \mathcal{C} for the deviations in molecule number (δX_i) is related to Ξ via the relation $\mathcal{C} = \Omega \Xi$. Thus, in the linear noise approach the expected value $\langle X_r \rangle$ is approximated by $\Omega \psi_r$ and the true covariance σ_{rp}^2 by c_{rp} . Then, the expressions for Pearson's correlation coefficients (ρ_{X_r, X_p}), Fano factors (f_X) and coefficients of variation (CV_X) can be easily derived:

$$\begin{aligned} \rho_{X_r, X_p} &= \frac{\sigma_{rp}^2}{\sigma_{rr} \sigma_{pp}} \sim \frac{c_{rp}}{\sqrt{c_{rr} c_{pp}}} = \frac{\xi_{rp}}{\sqrt{\xi_{rr} \xi_{pp}}}, \\ CV_{X_r} &= \frac{\sigma_{rr}}{\langle X_r \rangle} \sim \frac{\sqrt{c_{rr}}}{\Omega \psi_r} = \frac{\sqrt{\xi_{rr}}}{\psi_r}, \\ f_{X_r} &= \frac{\sigma_{rr}^2}{\langle X_r \rangle} \sim \frac{c_{rr}}{\Omega \psi_r} = \frac{\xi_{rr}}{\psi_r}. \end{aligned} \quad (24)$$

Therefore, thanks to Equation (23) the matrix \mathcal{C} (and thus the stochastic properties of a system) can be directly evaluated from macroscopic parameters.

Let's now discuss in details the specific case with two ceRNAs in interaction with one miRNAs. In such a system, the propensity vector f assumes the following form:

$$f := \{k_{S_1}, S_1 g_{S_1}, g_{11} S_1 R_1, g_{12} S_1 R_2, k_{S_2}, S_2 g_{S_2}, g_{21} S_2 R_1, g_{22} S_2 R_2, k_{R_1}, R_1 g_{R_1}, k_{R_2}, R_2 g_{R_2}\}, \quad (25)$$

and the stoichiometry matrix ν is given by:

$$\nu = \begin{pmatrix} 1 & 0 & 0 & 0 \\ -1 & 0 & 0 & 0 \\ -\alpha & 0 & -1 & 0 \\ -\alpha & 0 & 0 & -1 \\ 0 & 1 & 0 & 0 \\ 0 & -1 & 0 & 0 \\ 0 & -\alpha & -1 & 0 \\ 0 & -\alpha & 0 & -1 \\ 0 & 0 & 1 & 0 \\ 0 & 0 & -1 & 0 \\ 0 & 0 & 0 & 1 \\ 0 & 0 & 0 & -1 \end{pmatrix}. \quad (26)$$

Thus, the Jacobian and diffusion matrices (\mathcal{A} and \mathcal{B} respectively) follow,

$$\begin{aligned} \mathcal{A} &= \begin{pmatrix} -g_{S_1} - \alpha(g_{11}R_1 + g_{12}R_2) & 0 & -\alpha g_{11}S_1 & -\alpha g_{12}S_1 \\ 0 & -g_{S_2} - \alpha(g_{21}R_1 + g_{22}R_2) & -\alpha g_{21}S_2 & -\alpha g_{22}S_2 \\ -g_{11}R_1 & -g_{21}R_1 & -g_R - g_{11}S_1 - g_{21}S_2 & 0 \\ -g_{12}R_2 & -g_{22}R_2 & 0 & -g_R - g_{12}S_1 - g_{22}S_2 \end{pmatrix} \\ \mathcal{B} &= \begin{pmatrix} k_{S_1} + g_{S_1}S_1 + \alpha^2 S_1 A & 0 & \alpha g_{11}R_1 S_1 & \alpha g_{12}R_2 S_1 \\ 0 & k_{S_2} + g_{S_2}S_2 + \alpha^2 S_2 B & \alpha g_{21}R_1 S_2 & \alpha g_{22}R_2 S_2 \\ \alpha g_{11}R_1 S_1 & \alpha g_{21}R_1 S_2 & k_{R_1} + R_1 C & 0 \\ \alpha g_{12}R_2 S_1 & g_{22}R_2 S_2 & 0 & k_{R_2} + R_2 D \end{pmatrix}, \end{aligned} \quad (27)$$

with $A = g_{11}R_1 + g_{12}R_2$, $B = g_{21}R_1 + g_{22}R_2$, $C = g_{R_1} + g_{11}S_1 + g_{21}S_2$ and $D = g_{R_2} + g_{12}S_1 + g_{22}S_2$. The covariance matrix elements c_{rp} can be evaluated accordingly. In Figure 8 we plot the Pearson correlation coefficient of such system as a function of ceRNA1 transcription rate. As it is possible to notice, Gaussian approximation performs better than Linear Noise approximation [31].

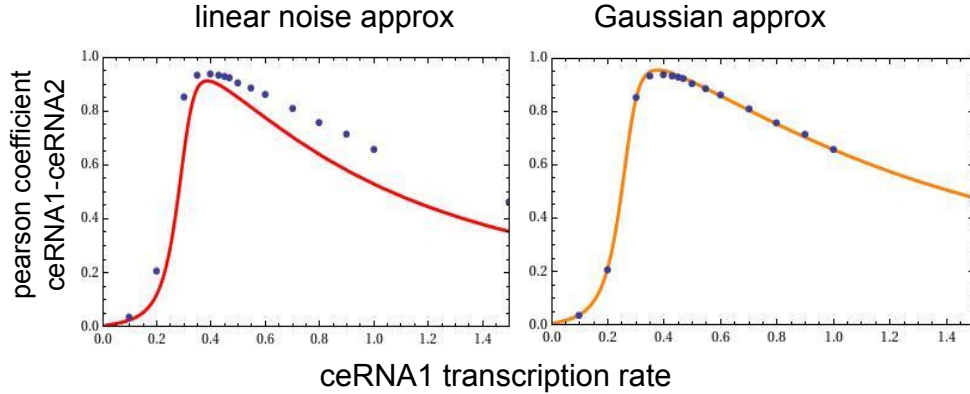


Figure 8. Comparison between Linear Noise and Gaussian approximations. (Left panel) Linear noise approximation, (Right panel) Gaussian approximation. Lines are analytical approximations of the Pearson correlation coefficient. Dots are the results of 10^4 Gillespie's simulations.

E Figure parameters (main text)

Figure 2

miRNAs transcription rates: $k_{S_1} = 0.05s^{-1}$ and $k_{S_2} = 0.045s^{-1}$;
 ceRNA2 transcription rate: $k_{R_2} = 0.155s^{-1}$;
 miRNA degradation rates: $g_{S_1} = g_{S_2} = 0.0002s^{-1}$;
 ceRNAs degradation rates: $g_{R_1} = g_{R_2} = 0.0004s^{-1}$;
 ceRNA-miRNA association rates: $g_{11} = g_{12} = g_{21} = g_{22} = 0.0005s^{-1}$;
 catalyticity parameter: $\alpha = 0.1$.
 ceRNA1 transcription rate is the control parameter and ranges from 0 to $1.4s^{-1}$.

Figure 3

miRNA2 transcription rate: $k_{S_2} = 0.03s^{-1}$;
 ceRNAs transcription rates: $k_{R_1} = 0.355s^{-1}$ and $k_{R_2} = 0.155s^{-1}$;
 miRNA degradation rates: $g_{S_1} = g_{S_2} = 0.0002s^{-1}$;
 ceRNAs degradation rates: $g_{R_1} = g_{R_2} = 0.0004s^{-1}$;
 ceRNA-miRNA association rates: $g_{11} = g_{12} = g_{21} = g_{22} = 0.0005s^{-1}$;
 catalyticity parameter: $\alpha = 0.1$.
 miRNA1 transcription rate is the control parameter and ranges from 0 to $0.1s^{-1}$.

Figure 4

Panel (B):

miRNA1-10 transcription rates: $k_S = 0.075 + 0.01\text{rand}()s^{-1}$;
 ceRNA2-10 transcription rate: $k_R = 0.15 + 0.01\text{rand}()s^{-1}$;
 miRNA1-10 degradation rates: $g_S = 0.0004s^{-1}$;
 ceRNAs1-10 degradation rates: $g_R = 0.0004s^{-1}$;
 miRNA-ceRNA association rates: $g = 0.0006$;
 catalyticity parameter: $\alpha = 0.5$.
 ceRNA1 transcription rate is the control parameter and every 35 hours takes the following values: $0.15s^{-1}$, $0.5s^{-1}$, $0.9s^{-1}$, $0.15s^{-1}$.

Panel (C):

miRNA1-9 transcription rate: $k_S = 0.02s^{-1} + 0.01\text{rand}()s^{-1}$;
 ceRNA1-10 transcription rates: $k_R = 0.15 + 0.01\text{rand}()s^{-1}$;
 miRNA1-10 degradation rates: $g_S = 0.0002s^{-1}$;
 ceRNA1-10s degradation rates: $g_R = 0.0004s^{-1}$;
 miRNA-ceRNA association rates: $g = 0.0006s^{-1}$;
 catalyticity parameter: $\alpha = 0.5$.
 miRNA1 transcription rate is the control parameter and every 35 hours takes the following values: $0.02s^{-1}$, $0.1s^{-1}$, $0.8s^{-1}$, $0.02s^{-1}$.

Figure 5

miRNAs transcription rates: $k_S = 0.2s^{-1}$;
 ceRNA2 transcription rate: $k_{R_2} = 0.155s^{-1}$;
 miRNA degradation rates: $g_{S_1} = g_{S_2} = 0.0003s^{-1}$;

ceRNAs degradation rates: $g_{R_1} = g_{R_2} = 0.0004s^{-1}$;
 complex association rates: $k_1^+ = k_2^+ = 0.0005s^{-1}$;
 complex dissociation rates: $k_1^- = k_2^- = 0.0003s^{-1}$;
 complex degradation rates: $\gamma_1 = \gamma_2 = 0.00031s^{-1}$;
 catalyticity parameter: $\alpha = 0.1$.
 ceRNA1 transcription rate is the control parameter and ranges from 0 to $1.2s^{-1}$.

Figure 6

ceRNA1 transcription rates: $k_{R_1} = 0.155s^{-1}$;
 ceRNA2_{OFF}→_{ON} transcription rate jumps from $k_{R_2} = 0$ to $k_{R_2} = 0.345$;
 ceRNA2_{ON}→_{OFF} transcription rate jumps from $k_{R_2} = 0.345$ to $k_{R_2} = 0$;
 miRNA degradation rates: $g_{S_1} = g_{S_2} = 0.0002s^{-1}$;
 ceRNAs degradation rates: $g_{R_1} = g_{R_2} = 0.0004s^{-1}$;
 ceRNA-miRNA association rates: $g_{11} = g_{12} = g_{21} = g_{22} = 0.0005s^{-1}$;
 catalyticity parameter: $\alpha = 0.1$.
 miRNA1 transcription rate is the control parameter and ranges from 0 to $0.5s^{-1}$. All the other ceRNAs have transcription rates $k_R = 0.1$ and all the other rates equal to ceRNA1 ones.

F Response time and experimentally testable trend

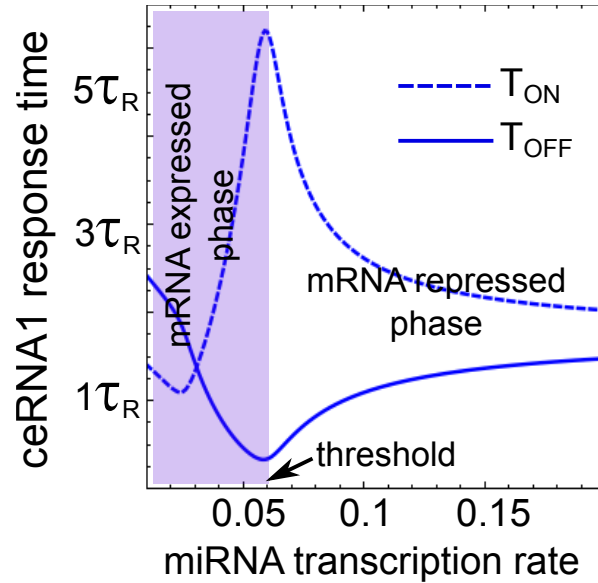


Figure 9. *Response times and experimentally accessible parameter region.* We show together the T_{ON} and T_{OFF} response times as present in Figure 6 in the main text for the case with 3 ceRNAs. The highlighted region corresponds to the experimentally accessible one. Increasing miRNA concentration, switch-off response times show a decreasing trend while switch-on a U-shaped one. The parameter setting is the same of Figure 6 (main text).

References

1. Anders Jacobsen, Jiayu Wen, Debora S. Marks, and Anders Krogh. Signatures of rna binding proteins globally coupled to effective microrna target sites. *Genome Research*, 20(8):1010–1019, 2010.
2. L Salmena, L Poliseno, Y Tay, L Kats, and PP Pandolfi. A cerna hypothesis: the rosetta stone of a hidden rna language? *Cell*, 146(5):353–358, 2011.
3. Y Tay, L Kats, L Salmena, D Weiss, SM Tan, U Ala, F Karreth, L Poliseno, P Provero, F Di Cunto, J Lieberman, I Rigoutsos, and PP Pandolfi. Coding-independent regulation of the tumor suppressor pten by competing endogenous mrnas. *Cell*, 147(5):344–357, 2011.
4. J. Winter, S. Jung, S. Keller, R.I. Gregory, and S. Diederichs. Many roads to maturity: microrna biogenesis pathways and their regulation. *Nature cell biology*, 11(3):228–34, 2009.
5. J. Krol, I. Loedige, and W. Filipowicz. The widespread regulation of microrna biogenesis, function and decay. *Nature Reviews Genetics*, 11(9):597–610, 2010.
6. H. Seitz. Redefining microrna targets. *Current Biology*, 19(10):870–873, 2009.
7. F.A. Karreth, Y. Tay, D. Perna, U. Ala, S.M. Tan, A.G. Rust, G. DeNicola, K.A. Webster, D. Weiss, P.A. Perez-Mancera, et al. In vivo identification of tumor-suppressive pten cernas in an oncogenic braf-induced mouse model of melanoma. *Cell*, 147(2):382–395, 2011.
8. Zina Jeyapalan, Zhaoqun Deng, Tatiana Shatseva, Ling Fang, Chengyan He, and Burton B. Yang. Expression of cd44 3'-untranslated region regulates endogenous microrna functions in tumorigenesis and angiogenesis. *Nucleic Acids Research*, 39(8):3026–3041, 2011.
9. P. Sumazin, X. Yang, H.S. Chiu, W.J. Chung, A. Iyer, D. Llobet-Navas, P. Rajbhandari, M. Bansal, P. Guarnieri, J. Silva, et al. An extensive microrna-mediated network of rna-rna interactions regulates established oncogenic pathways in glioblastoma. *Cell*, 147(2):370–381, 2011.
10. Erel Levine, Zhongge Zhang, Thomas Kuhlman, and Terence Hwa. Quantitative characteristics of gene regulation by small rna. *PLoS Biol*, 5(9)(9):e229, 08 2007.
11. Namiko Mitarai, Anna M C Andersson, Sandeep Krishna, Szabolcs Semsey, and Kim Sneppen. Efficient degradation and expression prioritization with small rnas. *Physical Biology*, 4(3):164, 2007.
12. Johan Elf, Johan Paulsson, Otto Berg, and Måns Ehrenberg. Near-critical phenomena in intracellular metabolite pools. *Biophysical Journal*, 84:154–170, 2003. Part of urn:nbn:se:uu:diva-4291.
13. N.E. Buchler and M. Louis. Molecular titration and ultrasensitivity in regulatory networks. *Journal of Molecular Biology*, 384(5):1106 – 1119, 2008.
14. Erel Levine and Terence Hwa. Small rnas establish gene expression thresholds. *Current Opinion in Microbiology*, 11(6):574 – 579, 2008. `jc:title;Growth and Development: Eukaryotes/Prokaryotes;ce:title;.`
15. Yishai Shimoni, Gilgi Friedlander, Guy Hetzroni, Gali Niv, Shoshy Altuvia, Ofer Biham, and Hanah Margalit. Regulation of gene expression by small non-coding RNAs: a quantitative view. *Mol Syst Biol*, 3:138, 2007.
16. S Mukherji, MS Ebert, GX Zheng, JS Tsang, PA Sharp, and A van Oudenaarden. Micrnas can generate thresholds in target gene expression. *Nature Genetics*, 43(5):854–859, 2011.

17. M. Kaern, T.C. Elston, W.J. Blake, and J.J. Collins. Stochasticity in gene expression: from theories to phenotypes. *Nat Rev Genet*, 6(6):451–464, 2005.
18. N. Maheshri and E.K. OShea. Living with noisy genes: how cells function reliably with inherent variability in gene expression. *Annu Rev Biophys Biomol Struct*, 36:413–434, 2007.
19. A. Raj and A. van Oudenaarden. Nature, nurture, or chance: stochastic gene expression and its consequences. *Cell*, 135:216–226, 2008.
20. Ugo Ala, Florian Karreth, Carla Bosia, Andrea Pagnani, Riccardo Taulli, Valentine Leopold, Yvonne Tay, Paolo Provero, Riccardo Zecchina, and Pier Paolo Pandolfi. Integrated transcriptional and cerna networks are cross-regulated in permissive molecular environments. *submitted*.
21. X. Li, J.J. Cassidy, C.A. Reinke, S. Fischboeck, and R.W. Carthew. A microrna imparts robustness against environmental fluctuation during development. *Cell*, 137(2):273–282, 2009.
22. M. Inui, G. Martello, and S. Piccolo. Microrna control of signal transduction. *Nat Rev Mol Cell Biol*, 11(4):252–263, 2010.
23. M.S. Ebert and P.A. Sharp. Roles for micrnas in conferring robustness to biological processes. *Cell*, 149(3):515–524, 2012.
24. G. Hutvagner and P. D. Zamore. A microrna in a multiple-turnover rnai enzyme complex. *Science*, 297(5589):2056–2060, 2002.
25. B. Haley and P.D. Zamore. Kinetic analysis of the rnai enzyme complex. *Nature structural & molecular biology*, 11(7):599–606, 2004.
26. J. Liu, F.V. Rivas, J. Wohlschlegel, J.R. Yates, R. Parker, and G.J. Hannon. A role for the p-body component gw182 in microrna function. *Nature cell biology*, 7(12):1261–1266, 2005.
27. R.S. Pillai, S.N. Bhattacharyya, C.G. Artus, T. Zoller, N. Cougot, E. Basyuk, E. Bertrand, and W. Filipowicz. Inhibition of translational initiation by let-7 microrna in human cells. *Science*, 309(5740):1573–1576, 2005.
28. Z.S. Kai and A.E. Pasquinelli. Microrna assassins: factors that regulate the disappearance of mirnas. *Nature structural & molecular biology*, 17(1):5–10, 2010.
29. A. Baccarini, H. Chauhan, T. J. Gardner, A. D. Jayaprakash, R. Sachidanandam, and B. D. Brown. Kinetic analysis reveals the fate of a microrna following target regulation in mammalian cells. *Current Biology*, 21(5):369–376, 2011.
30. N.G. van Kampen. *Stochastic processes in physics and chemistry*. North holland, 2007.
31. Louis Fernandez Lafuerza. Gaussian approximation to the resolution of master equations. Master’s thesis, Universitat de les Illes Balears, 2009.
32. E. Levine, M. Huang, Y. Huang, T. Kuhlman, H. Shi, Z. Zhang, and T. Hwa. On noise and silence in small rna regulation. Preprint, 2008.
33. Yue Hao, Yufang Xu, and Hualin Shi. Theoretical analysis of catalytic-srna-mediated gene silencing. *Journal of Molecular Biology*, 406(1)(1):195–204, 2011.
34. Carla Bosia, Matteo Osella, Mariama El Baroudi, Davide Cora, and Michele Caselle. Autoregulation via intronic micrnas and its functions. *BMC Systems Biology*, in publication, 2012.

35. D. Muzzey and A. van Oudenaarden. Quantitative time-lapse fluorescence microscopy in single cells. *Annual review of cell and developmental biology*, 25:301–327, 2009.
36. Daniel T. Gillespie. A general method for numerically simulating the stochastic time evolution of coupled chemical reactions. *Journal of Computational Physics*, 22(4):403–434, 1976.
37. H. Risken. *The Fokker-Planck equation: Methods of solution and applications*, volume 18. Springer Verlag, 1996.